Investigation of the hypoxia adaptation mechanisms in *Aspergillus fumigatus*

(病原真菌 *Aspergillus fumigatus* における低酸素適応機構に関する研究)

千葉大学大学院医学薬学府

先端医学薬学専攻

(主任：　石和田　稔彦教授)

BIAN CAI

Contents

Abstract

The filamentous fungus *Aspergillus fumigatus* is the most important pathogenic fungus in the genus *Aspergillus* and is associated with aspergillosis, which has caused a high mortality rate among immunocompromised patients, primarily due to limited antifungal therapies. *A. fumigatus* must adapt to a hypoxic microenvironment to survive and thrive in the human hosts. Several mechanisms related to hypoxia adaptation in *A. fumigatus* have been elucidated. To gain deeper insights into this adaptation, a laboratory passaging experiment was performed using six *A. fumigatus* clinical strains, each with different hypoxia fitness.

After a 20-generation passaging under the hypoxic environment (1% oxygen), a laboratory-evolved strain harboring hypoxia fitness (Afs35-G20) was generated, and a mutation in the Ras-GAP encoding gene, *AfgapA*, was identified with the application of whole genome sequencing. This mutation could result in the deletion of 22 amino acids at the C-terminus of AfGapA. AfGapA shares high similarity with Ras-GAP orthologs in other phylogenetically close related fungi, such as *A. nidulans*. Ras-GAP down-regulates the activity of Ras proteins by participating in the Ras-mediated pathways, which control a variety of morphogenetic processes in fungi. Ras in *C. neoformans* has been proved necessary for its hypoxia fitness. However, the Ras-GAP encoding gene has not been uncharacterized yet in *A. fumigatus,* and the role of Ras in hypoxia fitness is poorly understood.

To investigate the functions of AfGapA, I constructed Afs35-G20 harboring wild type *AfgapA* (Afs35-G20-$AfgapA^{WT}$), and the *AfgapA* null mutant (Δ*AfgapA*). Relevant phenotypes were then compared among the two AfGapA wild type strains, i.e., Afs35 and Afs35-G20-$AfgapA^{WT}$, and the two AfGapA mutant strains, i.e., Afs35-G20 and Δ*AfgapA*. As a result, the hypoxia fitness of Afs35-G20 was reversed by introducing $AfgapA^{WT}$. Two AfGapA mutant strains exhibited reduced conidiation, yellowish pigmentation, abnormal cellular polarity and increased fungal virulence. Moreover, the AfGapA dysfunction contributes to fungal virulence in silkworm model. Δ*AfgapA* exhibited more severe phenotypes than Afs35-G20, such as relatively reduced conidiation and higher virulence level, indicating that the *AfgapA* mutation in Afs35-G20 may be a partial loss-of-function due to the truncation of the proteins at the C-terminus.

In conclusion, *AfgapA* dysfunction may lead to the downregulation of its Ras substrate(s), reflecting several phenotypes such as increased hypoxia fitness, hypervirulence, poor conidiation and conidial pigmentation. Here, this study reports the function of a Ras-GAP protein encoding gene *AfgapA* in *A. fumigatus* for the first time.

Introduction

Aspergillus fumigatus is an opportunistic pathogen that causes aspergillosis, a disease that causes invasive pulmonary aspergillosis (IPA), pulmonary aspergilloma, and allergic bronchopulmonary aspergillosis. IPA, in particular, has a high mortality rate (Denning 1998). The development of an effective therapy of aspergillosis has proven to be difficult because of the limited antifungal drugs and the prevalence of antifungal-resistant strains worldwide (Howard et al. 2009). J.-P Latge *et al.* reported that *A. fumigatus* is the most important aerial fungal pathogen to date (Latgé and Chamilos 2019). The number of immunocompromised patients in worldwide is increasing rapidly, and *A. fumigatus* has become a leading cause of mortality in this patient population (Latgé 1999; Latgé 2001). Depending on the immune status and other factors of the patients, mortality rates is associated with invasive aspergillosis range from 60 to 90% (Brakhage and Langfelder 2002).

A. fumigatus propagates by producing conidia, which easily disperse into the air. Conidia are present in indoor and outdoor environments at concentrations ranging between 1 and 100 conidia per m^3; however, this can increase up to 10^8 conidia per m^3 in certain environments; for example, in composting plants found in the agricultural production (Wery 2014). *A. fumigatus* causes diseases in human beings through the inhalation of airborne conidia into lungs. Humans inhale hundreds of conidia during daily life, but they can be eliminated efficiently by immune system in healthy people (Latgé 2001). However, conidia can germinate and grow in the immunocompromised patients, and eventually causes diseases.

A. fumigatus must face and overcome a variety of in vivo challenges once it is inhaled by a human host. Thus, investigating how fungi adapts to these challenging microenvironments *in vivo* is important for understanding *A. fumigatus* pathogenicity. However, we still have lacking knowledge about how *A. fumigatus* survives and thrives in the microenvironments in the human lung. Hypoxia, which is, low levels of oxygen, has been proven to exist not only in soil and compost heaps, but also in human lungs to which *A. fumigatus* conidia are exposed (Fig. 1). It has been reported that in humans, various factors such as tissue type and inflammatory response can influence the oxygen level. Oxygen levels in most tissues are found to be remarkably below atmospheric levels (21%) (Studer et al. 2000; Carlsson et al. 2001; Erecińska and Silver 2001). Even in the alveoli of healthy lungs, which is the most oxygen rich organ, the oxygen level is at a mere 14%. After oxygen reaches the capillaries and diffuses into the surrounding tissues, the concentration decreases further to 2–4% (Warn 2004). Moreover, it is reported that at sites of inflammation, available oxygen is significantly reduced compared to surrounding tissues (van Belle et al. 1987; Matherne et al. 1990; Dewhirst 1998). Besides, in inflamed tissues, the blood supply is often restricted because the vessels are congested with phagocytes or the pathogen itself (Simmen et al. 1994). Thus, it is conceivable that hypoxic microenvironments are generated

during fungal infiltration.

Hypoxic microenvironments have been confirmed in the sites of local tissues in experimental models of *A. fumigatus* infection (Schrettl et al. 2010). During infection, the continuous activation of the inflammatory response contributes to further development of hypoxia due to the destruction of the pulmonary tissue as collateral damage (Fliesser et al. 2015). Therefore, it is highly probable that *A. fumigatus* has evolved strategies to adapt to hypoxic environments. Indeed, Kowalski et al. reported a strong correlation between hypoxia fitness and *A. fumigatus* virulence (Kowalski et al. 2016).

Various mechanisms of sensing and responding to hypoxia have been reviewed in yeast and pathogenic fungi (Bien and Espenshade 2010; Grahl et al. 2012b; Siso et al. 2012; Butler 2013). In *A. fumigatus,* the master transcriptional regulator of the hypoxic response, SrbA, is essential for both its growth in hypoxia in vitro and for its virulence in vivo (Willger et al. 2008, 2012). Transcriptome analysis indicates that SrbA is associated with a broad range of biological processes including: ergosterol biosynthesis, iron homeostasis, cell wall biosynthesis, amino acid biosynthesis, general carbon metabolism, and the GABA shunt (Barker et al. 2012). Additionally, certain enzymes and proteins that contribute to fungal virulence are exclusively secreted under hypoxic conditions (Grahl et al. 2011; Hillmann et al. 2014; Bat-Ochir et al. 2016; Vaknin et al. 2016; Kroll et al. 2016). Furthermore, mitochondrial respiration has been proved to be active in hypoxia, and alternative oxidase (*aoxA)* and cytochrome C (*cycA*) are essential for hypoxic tolerance and pathogenesis (Grahl et al. 2012a). These findings imply that multiple pathways are involved in oxygen sensing and hypoxia responses in *A. fumigatus*.

A previous study (Kowalski et al. 2016) investigated the morphology of hypoxia-adapted *A. fumigatus* strains by performing the laboratory passaging, and identified a furrow morphology in plate culture caused by the exposure to hypoxic environments. They subsequently identified *hrmA* to be responsible for the morphological changes that occurred in the hypoxia adapted strains. Furthermore, they identified hrmA-associated cluster (HAC) with the application of transcriptomic analysis. However, the presence of HAC seemed to be genetically heterogeneous (Kowalski et al 2009; Barber et al 2021). These observations suggest the presence of other mechanisms of hypoxia adaptation in *A. fumigatus*. To further investigate the mechanism of hypoxia adaptation in a more general scope, it is required to identify the factors that are widely conserved among *A. fumigatus* strains.

To this end, I performed a laboratory passaging experiment using six *A. fumigatus* clinical strains, which have different hypoxia fitness in plate culture. Consequently, a hypoxia adapted strain, Afs35-G20, was then generated. Afs35-G20 exhibited decreased colony growth in both hypoxia and normoxia, but possessed increased hypoxia fitness in liquid culture. Seeking the causal mutations in Afs35-G20, a nonsense mutation in *AfgapA* (Tyr757Ter) encoding a Ras-

GAP protein was identified, which could result in the deletion of 22 amino acids at the C-terminus. The hypoxia fitness of Afs35-G20 in liquid culture was reversed by introducing wild type *AfgapA*. Moreover, Δ*AfgapA* exhibited greater hypoxia fitness and a hypervirulent phenotype. I conclude that *AfgapA* may be responsible for hypoxia fitness, particularly in liquid cultures, conceivably through the overactivation of Ras proteins. Taken together, the dysfunction of *AfgapA* may be followed by the downregulation of its Ras substrate(s), reflecting several phenotypes, such as increased hypoxia fitness, hypervirulence, poor conidiation and conidial pigmentation. This study reports the function of a Ras-GAP protein *AfgapA* in *A. fumigatus* for the first time.

Materials and methods

Strains and media

The 56 *A. fumigatus* clinical strains used to investigate the hypoxia adaptation in this study are listed in Table S1. The 56 strains are highlighted with blue-colored nodes in the whole-genome SNP-based tree of 174 *A. fumgiatus* strains (Fig. S1), which were deprived from an unpublished study. Strains further used and generated based on Afs35 and Afs35-G20 are listed in Table 2. All strains were stored as conidial suspensions in 50% glycerol at −80 °C. Strains were grown on 1% glucose minimal medium (GMM) (Shimizu and Keller 2001) at 37 °C, and conidia were collected in 0.8% NaCl and 0.1% Tween for *in vitro* assays. For silkworm infection, conidia were collected in 0.54% NaCl and 0.05% Tween. For all solid media, 1.5% agar was added before autoclaving.

Serial passaging of six *A.fumigatus* clinical strains under the low-oxygen conditions

Serial passage experiments were performed as described by a previous study (Kowalski et al. 2016) with slight modifications. This study used *A. fumigatus* Af293, Afs35, IFM 58401, IFM 59365, IFM 63559, and IFM 63240 as parental strains. Briefly, each strain was grown for four days at 37 °C in 1% oxygen on GMM without $FeSO_4 \cdot 7H_2O$ to mimic the oxygen- and nutrient-poor microenvironment of the host. The conidia were then subcultured/passaged for 20 generations for a total of 80 days in hypoxia (Fig. 3A). Subsequently, the single spore was isolated from the G20 conidia population. Hypoxic conditions were maintained by using a multi-gas incubator (MG-71M, TAITEC, Saitama, Japan).

Microsatellite genotyping

Short tandem repeats (STRs) from Afs35 and the two single isolated colonies of Afs35-G20 were obtained using previously described methods (Hagiwara et al. 2014). Nine microsatellite regions of approximately 400 bp were PCR amplified using appropriately designed primer pairs and sequenced using Sanger sequencing. The repeat numbers of each locus were then counted from the sequences. STRs from G5s and G20s of other strains were obtained from *de novo* assembly data using a customized Python script (Fig. S2).

Growth assays and stress tests

Conidia were harvested from five-day-old cultures on GMM plates inculated at 37 °C. The number of conidia in the suspensions was counted using a hemocytometer (Watson, Kobe, Japan). Growth diameter was quantified by point inoculating 1×10^3 conidia on GMM plates at 37 °C under normoxic (~21% oxygen) and hypoxic (1% oxygen) conditions. Colony diameter

was measured after four days and reported as the average of three biological replicates per strain. Fungal biomass was quantified by measuring the dry weight of fungal tissue from 5×10^7 conidia grown in 100 mL of liquid GMM with shaking at 200 rpm for 48 h, under both normoxic and hypoxic conditions. The liquid biomass was reported as the average of three biological replicates per strain.

For the cell wall perturbing agents analysis, 1 mg/mL Congo red (CR) (Sigma; catalog no. C6277) was used. For the copper-sensing assays, 100 μM CuSO4 (copper-repleted) and 100 μM bathocuproinedisulfonic acid (BCS) (copper-depleted) were used, and 1×10^3 conidia were inoculated in each condition. Colony diameter was measured after four days and reported as the average of three biological replicates per strain. Diameter ratio was calculated as the diameter in GMM with corresponding agent, to that in plain GMM plate. Images are representative of three biological replicates.

Construction of the reconstituted and disruptive strains

The construction of the reconstituted and disruptive strains of *AfgapA* were performed by using the CRISPR/Cas9 system (Umeyama et al. 2018). Primers used for the strain construction in are presented in Table 4. First, the *hph* (hygromycin B resistance cassette) was amplified from the pHph plasmid, after which the repair templates were constructed by PCR sewing and overlap extension PCR for both the reconstituted strain and the disruptive strain.

For the reconstituted strain, fragments A and B, representing the upstream region of *AfgapA* and partial *AfgapA,* respectively, were amplified from the genomic DNA of Afs35-G20 using the primer sets of primer no. 1 (3g09900-UF) + primer no. 2 (3g09900-sg5Mut-UR) and primer no. 3 (3g09900-sg5Mut-M1F) + primer 4 (3g09900-G_T-sg3Mut-M1R), respectively. Fragment C, which were partial *AfgapA* and around 720 bp downstream regions of *AfgapA,* was amplified using primer sets primer no. 5 (3g09900-G_T-sg3Mut-M2F) + primer no. 6 (Hph-3g09900-M2R), respectively. Primer no. 4 and primer no. 5 contained the wild type of *AfgapA.* Lastly, fragment D was amplified using primer no. 7 (Hph-3g09900-DF) + primer no. 8 (3g09900-DR). Primer no. 6 and primer no. 7 contained a 24 bp sequence complementary to the *hph* sequences at the 5′ end (blue fragments in Fig. 17A). Subsequently, recombinant PCR was performed to fuse fragments A, B, C, *hph*, and D through overlap extension PCR, followed by transformation (Fig. 17A).

For the disruptive strain, fragment E and F corresponding to about 1kbp upstream and downstream regions of *AfgapA*, respectively, were amplified from the genomic DNA of Afs35 by using the primer sets of primer no. 1 + primer no. 9 (Hph-3g09900-UR) and primer no. 10 (Hph-3g09900-DF) + primer no. 11 (3g09900-DR_deletion), respectively. Primer no. 9 and primer no. 10 contained a 24 bp complementary to *hph* sequences at the 5′ end. Then, recombinant PCR was

performed to fuse fragments E, *hph,* and F by overlap extension PCR (Fig. 17B).

Subsequently, the transformation was performed. Transformation of *A. fumigatus* was performed according to Umeyama's method for genome editing using CRISPR/Cas9 (Umeyama et al. 2018). The culture and protoplast solution were prepared according to previous studies (Szewczyk et al. 2006; Umeyama et al. 2018). Briefly, conidia were incubated at 37 ºC in 10 mL of YG medium [5 g yeast extract (BD Difco, MD, USA), 20 g D-glucose and 400 µL of trace elements in 1L distilled water] for 5–6 h. Ten mL of protoplast solution containing 4 g VinoTaste Pro (Novozymes, Bagsvaerd, Denmark) was supplemented in the culture for generating protoplasts. The transformants were screened by CZAPEK DOX BROTH (CDB: Duchefa Biochemie, Haarlem, Netherlands) agar supplemented with 1 M sucrose containing 400 µg/mL hygromycin B. The successful transformants were selected by PCR of the inserted fragments, followed by verification of the sequences of all amplified fragments using the ABI 3130xl Genetic Analyzer (Thermo Fisher Scientific, MA, USA) (partial is shown in Fig. 18).

RNA extraction and quantitative real-time RT-PCR

Mycelia of Afs35, Afs35-G20, and Δ*AfgapA* were harvested after growth in GMM liquid media at 37ºC for 24 h. Total RNA was prepared by using a RNeasy Mini Kit (Qiagen, Hilden, Germany), and a cDNA was synthesized by reverse transcription using a RevaTra Ace qPCR RT Master Mix with gDNA remover (TOYOBO, Osaka, Japan).

Quantitative real-time RT-PCR analysis was performed on a LightCycler 96 Real-Time PCR System (Roche Diagnostics, Basel, Switzerland) with a THUNDERBIRD SYBER qPCR Mix (TOYOBO). The act1 gene was used as an internal control for quantification of the target gene expression. The relative expression ratio relative to that of Afs35 mycelia grown in GMM liquid media after 24 h post-inoculation was calculated using the $2^{-\Delta\Delta Ct}$ method. The primers used for real-time RT-PCR in this study are listed in Table 5.

Microscopic observation of conidia and hyphae

After liquid culture in GMM, the germinated conidia, or hyphae were sandwiched between cover glasses and glass slides. Morphology was observed and photographed using a Nikon ECLIPSE Ni microscope (Nikon, Tokyo, Japan), or a Shimadzu BA210E microscope (Shimadzu, Kyoto, Japan).

Calculation of conidia numbers

Three mL of GMM agar medium containing 1×10^4 conidia/mL was poured into a 6-well plate (Hagiwara et al. 2013). After incubation for 5 days at 37°C, the agar including mycelia and conidia was vortexed in a 5 mL of solution containing 0.8% NaCl and 0.1% Tween 80 for 3 min

to collect the conidia, and the conidia were counted by using a hemocytometer. Conidiation level is represented as the average from three biological replicates per strain.

Antifungal Susceptibility Testing

Antifungal susceptibility testing was performed as described previously (Hagiwara et al. 2018a). In brief, I performed tests using micafungin (MCFG), caspofungin (CPFG), 5-fluorocytosine (5-FC), fluconazole (FLCZ), amphotericin B (AMPH), itraconazole (ITCZ), voriconazole (VRCZ), and miconazole (MCZ) in RPMI 1640 medium (pH 7.0) at 35 ℃, according to the Clinical and Laboratory Standards Institute reference method for broth microdilution (https://clsi.org/standards/products/microbiology/documents/m38), with partial modifications using the dried plate for antifungal susceptibility testing (Eiken Chemicals, Tokyo, Japan).

Survival analysis

Virulence was assessed using the silkworm model. Silkworm (*Bombyx mori*) larvae were infected with *A. fumigatus* conidia with slight modifications of previous studies (Yu et al. 2021; Majima et al. 2021). Fifth star silkworms were purchased from Ehime Sansyu (Ehime, Japan). They were then raised at 25 °C for 2–3 days. The inoculum of 0.05 mL diluted to 3×10^6 conidia/mL, or 3×10^7 conidia/mL was injected into the hemolymph of silkworms using a 1 mL Terumo Myjector 29G insulin syringe (Terumo, Tokyo, Japan). After the infection, silkworms were maintained at 34 °C and their survival was evaluated using the Kaplan-Meier method using the survival package from the R programming language (https://www.r-project.org/).

Whole genome sequencing analysis

Genomic DNA was extracted from overnight cultured mycelia using the phenol-chloroform method as described previously (Takahashi-Nakaguchi et al. 2015). Genomic DNA libraries of *A. fumigatus* strains were constructed using an NEBNext Ultra DNA Library Prep Kit (New England BioLabs, Ipswich, MA, USA) according to the manufacturer's protocol. A 150-bp paired-end sequencing on a HiSeq X Ten system (Illumina, San Diego, CA, USA) was conducted by GENEWIZ (Suzhou, China).

Raw genomic reads were quality-controlled and trimmed using fastp (ver. 0.20.1) (Chen et al. 2018). The reference genome, Af293, was retrieved from FungiDB (http://fungidb.org/fungidb/) (Stajich et al. 2012). The filtered reads were aligned against the reference genome using BWA-MEM (ver. 0.7.17-r1188) (Li 2013). The single-nucleotide polymorphism (SNP) analysis was performed using SAMtools (ver. 1.10) (Li et al. 2009), and an in-house python script (Hagiwara et al. 2014). The alignment was visualized using IGV

(Integrative Genomics Viewer) (Thorvaldsdottir et al. 2013).

For the *de novo* assembly of Afs35 and Afs35-G20, the mitochondrial genomes were assembled using GetOrganelle (ver. 1.6.4) (Jin et al. 2020) with the trimmed reads. To filter the mitochondrial reads, the trimmed reads were aligned against the mitochondrial genomes by BWA (ver. 0.7.17-r1188) (Li 2013), and the mapped reads were filtered using SAMtools (ver. 1.10) (Li et al. 2009) and SeqKit (Shen et al. 2016). Filtered reads from the nuclear genome were used to assemble the nuclear genomes using SPAdes (ver. 3.14.0) (Bankevich, A., Nurk et al. 2012) with the options '--cov-cutoff auto' and '--careful'. For other strains, short reads filtered by fastp were directly assembled using SPAdes.

Prediction of the tertiary protein structure

The graphical representation of AfGapA, THTA and their mutants were depicted using IBS (ver. 1.0.3) (Liu et al. 2015). The tertiary protein structures were predicted using AlphaFold (ver. 2.0) with default parameters (Jumper et al. 2021), and then depicted and aligned using PyMol (DeLano 2002). pLDDT score (a per-residue measure of local confidence on a scale from 0 - 100) for each predicted protein structure was obtained from the AlphaFold models with the best score.

Phylogenetic analysis

The amino acid sequences of Ras-GAP in *A. fumigatus, A. nidulans, S.cerevisiae,* and *S. pombe* were obtained from FungiDB and aligned using MAFFT (ver. 7.475) (Katoh 2002; Katoh and Standley 2013). Four characteristic amino acid blocks of Ras-GAPs were visualized using MAFFT. The amino acid sequences of approximately 200 AfGapA orthologs were obtained from OrthoMCL (Li et al. 2003), and aligned using MAFFT. Gblocks was used to extract conserved regions from the multiple sequence alignment (Castresana 2000). After manual curation, 155 amino acid sequences were used for the phylogenetic analysis. A phylogenetic tree was constructed using multithreaded RAxML (ver. 8.2.12) (Stamatakis 2014), the PROTGAMMAWAG model, and 100 bootstrap replicates. The phylogenetic tree was visualized and edited using ggtree package in R (Yu et al. 2017).

Results

Serial passaging of six *A. fumigatus* clinical strains was conducted

The diameter of colony growth was measured in both hypoxia and normoxia of 56 *A. fumigatus* clinical strains. The detailed information of them is listed in Table S1. The ratio of the diameter of the colony in hypoxia and in normoxia (H/N diameter ratio) for each strain (Table S1, Fig. 2) was then calculated, which ranges from 0.12 to 0.93. Consequently, six *A. fumigatus* strains, i.e., Af293, Afs35, IFM 58401, IFM 59365, IFM 63559 and IFM 63240, which have different H/N diameter ratio (blue circles in Fig. 2), were selected for the following laboratory passage experiments. Among which, Afs35 is a non-homologous end joining deficient strain by deleting the $akuA^{KU70}$, as the parental strain (Ries et al. 2019; Bertuzzi et al. 2021).The workflow of the laboratory passaging experiment is depicted in Fig. 3A. Afterwards, the 5^{th}, 10^{th}, $15^{th,}$ and 20^{th} generation of each strain were investigated, and hereafter designated as G5, G10, G15 and G20, respectively.

A whole-genome analysis was performed for G5, G10, G15 and G20 of six investigated strains. Af293-based alignment and *de novo* assembly were then performed. Detailed information is listed in Table S2. Microsatellite analysis of short tandem repeats (STRs) is a recently developed genotyping method for the genetic discrimination of *A. fumigatus* strains (de Valk et al. 2005; Klaassen 2009). To determine whether the generated strains from passaging were genetically identical to their parental strain, microsatellite analysis was performed. STR regions of each strain were extracted and the number of STRs was counted from the *de novo* assembly using a customized Python script (Fig. S2). As a result, the STRs of G5 and G20 of IFM 63559 and IFM 63240 were inconsistent (Table S3), indicating a contamination may be occurred during the passaging experiment. The following experiments were, thus, conducted on the other four strains.

For the remaining four strains, the growth of G5s and G20s in hypoxia and normoxia were then evaluated and compared in plate culture. The colony phenotype was characterized for each G5 and G20 under the hypoxic and normoxic conditions (Fig. 4). To evaluate the hypoxia fitness in plate culture, colony diameter was measured. As a result, colony growth was comparable to their parental strains for most strains, except for Af293-G20, which exhibited an increased colony growth in hypoxia ($p = 0.02$). To evaluate the hypoxia fitness in liquid culture, the dry weight of fungal biomass in both hypoxia and normoxia were measured for G5s and G20s of each strain. The workflow is depicted in Fig. 3B. As a result, only Afs35-G20 exhibited increased biomass in hypoxia (deep grey bar in Fig. 5A). To account for the ability to grow in hypoxia relative to normoxia, I further calculated the ratio of biomass in hypoxia to that in normoxia (H/N fitness ratio) for each strain. The result appeared to be consistent to the biomass weight in hypoxia, that only Afs35-G20 exhibited an increment in hypoxia fitness in liquid culture (deep grey bar in

Fig. 5B).

Afs35-G20 exhibited increased hypoxia fitness in liquid culture

Single colony isolation was then performed for the conidia population of four G20 strains. As a result, there proved to be two colonies, colony1 and colony2 in the colony population of Afs35-G20, which exhibited different morphologies in plate culture. The morphology of colony 1 in plate culture was similar to that of Afs35, exhibited more fluffy, white hyphae, and comparable colony growth, whereas the other isolate produced less hyphae and impaired colony growth (Fig. 6A). In contrast, the other strains seemed to have only single colonies. Microsatellite analysis indicated that both colonies were genetically identical to their parental strain Afs35 (Fig. 6B). Colony 1 exhibited similar hypoxia fitness compared to the parental strain (Figs. 6C and 6D), whereas colony 2 exhibited an increased biomass production in hypoxia (Figs. 6E and 6F). Thus, colony 2 was hereafter designated as Afs35-G20 and further investigated. It could be concluded that among the four tested strain sets, Af293-G20 exhibited increased fitness in both hypoxia and normoxia in plate culture, but not in liquid culture. In contrast, Afs35-G20 has increased hypoxia fitness in liquid culture, although its colony growth was considerably impaired (Figs. 7A and 7B). Since Afs35-G20 exhibited increased H/N ratio in terms of both plate culture and liquid culture (Figs. 7C and 6F), the following investigations were exclusively focused on Afs35 and Afs35-G20.

Being a major and unique organelle of the fungal cell, the cell wall can protect *A. fumigatus* from external stimuli. It has been reported that *A. fumigatus* reshapes its fungal cell wall structure under hypoxic condition by increasing the hyphal cell wall thickness or altering the actin or beta-glucan component in the cell wall, which consequently influences various immune responses in the host (Shepardson et al. 2013). To this end, the cell wall integrity of the hypoxia adapted strain, Afs35-G20, was tested using a cell wall perturbing agent, Congo red (CR). As a result, Afs35-G20 exhibited higher tolerance to CR (Fig. 8A), strongly indicating that the cell wall component of Afs35-G20 could be changed along with the hypoxia adaptation.

Metals such as copper (Cu) and iron (Fe) are essential micronutrients for all organisms including pathogenic fungi (Andreini et al. 2008). Copper serves as a critical cofactor for numerous proteins in fungi (Robinson and Winge 2010; Festa and Thiele 2011). To evaluate whether the copper homeostasis of *A. fumigatus* was affected during the passaging in a nutrient-poor microenvironment, the susceptibility to both excess and deficiency of copper was tested by measuring the colony growth under the respective stimuli. Evidently, Afs35-G20 exhibited more susceptibility to high concentration of copper, but remained stable in the copper depletion condition (Fig. 8B), indicating that the copper export regulation may be impaired in Afs35-G20, but not the copper uptake regulation.

Mutation in a Ras-GAP encoding gene was identified in the hypoxia adapted strain

To gain further insight into the phenotypic difference between Afs35 and Afs35-G20, the whole-genome sequencing was re-conducted. Mutation identification based on mapping and *de novo* assembly were performed. The mapping rates in the reference genome (Af293, 29.4 Mb) were 98.14% and 98.35%, respectively. Seeking the mutations in Afs35-G20, three mutations were identified, including two SNPs and one two-base deletion (Table 1). According to the annotation, two of these were non-synonymous mutations resided within the coding region of the genes Afu3g09900 and Afu1g03992 (*thtA*), respectively. The assembly-based SNP calling result was consistent with the mapping-based results. The mutations in Afu3g09900 and *thtA* were confirmed using Sanger sequencing (data not shown). According to the mapping result visualization, the mutation in gene Afu3g09900 appeared after Afs35-G10, while the mutations in *thtA* and *dml1* appeared after Afs35-G15 (Fig. 10). In addition, two SNPs causing missense mutations were identified in other two strains, i.e., Af293-G20 and IFM 59365-G20, when compared to their parental strains (IGV snapshots were shown in Fig. S3). In contrast, no mutations were identified in IFM 58401-G20, which is consistent with its unchanged morphology in both plate and liquid culture.

I then focused on investigating the uncharacterized gene carrying the non-synonymous mutation, Afu3g09900. According to FungiDB, Afu3g09900 is annotated as an ortholog to GTPase activating protein (GAP) encoding genes. The 779-residue AfGapA polypeptide contains N-terminal RasGAP (PF00616) and C-terminal RasGAP_C (PF03836) PFAM domains characterizing regulatory proteins that accelerate the intrinsically slow GTPase activity of Ras protein family members (Fig. 11A). The substitution from T to G resulted in a nonsense mutation, Tyr757Ter in AfGapA, causing a 22 amino acid deletion adjacent to the domain RasGAP_C (Fig. 11A).

The structural bases of human H-Ras GTPase activity stimulation by a cognate GAP are well understood, which have four characteristic amino acid sequence blocks (Scheffzek et al. 1997). I performed the amino acid sequence alignment for AfGapA and other four sequences from its close relatives, including *A. nidulans* (GapA, AAO38800), *S. pombe* (Sar1, NP_595370) and *S. cerevisiae* (Sc IRA1, P18963 and Sc IRA2, CAA99093), all whose GAP proteins are already functionally characterized (Tanaka et al. 1990; Wang et al. 1991; Harispe et al. 2008). Indeed, AfGapA shares its domain organization in 92.6%, 44.4%, 24.4%, and 25.7% amino acid sequence identity, with GapA, Sar1, Sc IRA1and Sc IRA2 respectively. Thus, Afu3g09900 was designated as *AfgapA*. The four amino acid sequence blocks in Ras GAPs were indicated in boxes in Fig. 14. The presence of the four motifs in AfGapA implies catalytically active Ras-GAPs, including the "Arg finger" residue, which is proven to be critical in promoting GTP hydrolysis by H-Ras

(Scheffzek et al. 1997). This strongly suggests that the physiological role of AfGapA is to stimulate the GTPase activity of Ras protein(s) in *A. fumigatus*.

In addition, the other non-synonymous mutation is resided within *thtA*, which encodes a thermotolerance protein that is essential for the growth of *A. fumigatus* at high temperatures.

Tertiary structure prediction and phylogenetic analysis

To evaluate the effect of the 22 amino acid deletion adjacent to the RasGAP_C domain of AfGapA, the tertiary structure prediction was performed using AlphaFold 2.0; which showed a positional shift in the structure of the domain region, RasGAP_C (marked red in Fig. 11B) because of the truncation (marked yellow in Fig. 11B), whereas the other domain, RasGAP did not exhibit any positional shifts (marked blue in Fig. 11B). These structural changes of AfGapA observed in Afs35-G20 may contribute to its adaptation to hypoxic conditions and other phenotypic changes.

Additionally, tertiary structure of the other non-synonymous mutation in *thtA*, was also analyzed. According to the re-prediction by AUGUSTUS (ver. 3.3.3) (Stanke et al. 2006), the two-base deletion resulted in a frame shift of *thtA*, causing a 23 amino acid deletion in the middle region of THTA (Fig. 12A). According to the FungiDB and structure prediction result, the deletion was neither resided within any protein domain regions, nor caused any structural changes (Figs. 12A and 12B). To further evaluate the mutation in *thtA*, I examined the growth test at 48 °C. Afs35-G20 did not show any growth at 48 °C, whereas Afs35 did show growth (Fig. 9), indicating that the mutation of *thtA* could be responsible for the susceptibility to high temperatures. The predicted local difference distance test (pLDDT) scores (Mariani et al. 2013) of each model were also obtained from the top ranked prediction, which measure the confidence in the predicted structures (Fig. 13 and Fig. S4). The average score was approximately 79 and 83, for AfGapA and THTA, respectively, which was supposed to be modelled well, according to EMBL-EBI (https://www.ebi.ac.uk) (Cantelli et al. 2022).

To understand if the Ras-GAP protein is conserved among other fungi, a phylogenetic analysis was performed. A phylogenetic tree based on 155 amino acid sequences in the ortholog group OG6_109756 indicated that Ras-GAP is highly conserved across the fungal kingdom, including Ascomycota, Basidiomycota, and Mucoromycota (Fig. 15). Interestingly, I observed that the most of species seemed to have a single copy of Ras-GAP, especially those in Ascomycota, except for *S. cerevisiae*. The gene duplication of Ras-GAP mostly occurs in the division Mucoromycota (*Mucor circinelloides, Mucor lusitanicus, and Phycomyces blakesleeanu*s), Glomeromycota (*Rhizophagus irregularis*), and Basidiomycota (*Pleurotus ostreatus* and *Puccinia striiformis*) (colored nodes indicated in Fig. 15).

***AfgapA* dysfunction contributes to hypoxia fitness in liquid culture**

To investigate whether AfGapA^{Tyr757Ter} contributes to the phenotypic changes in Afs35-G20, I constructed Afs35-G20 harboring a wild-type *AfgapA*^{WT}, that is, Ter757Tyr, referred to as Afs35-G20-*AfgapA*^{WT}, using the CRISPR/CAS-9 gene-editing method (Umeyama et al. 2018). Two independent strains of the reconstituted strain were constructed and isolated, and their experimental results were similar. Thus, for simplicity, the result of only one of them will be shown in the rest of this study, if indicated otherwise. In addition, to address whether AfGapA mutation in Afs35-G20 represents a complete loss-of-function mutation, a *AfgapA* deletion strain, referred to as Δ*AfgapA* was also constructed. Strains further investigated in this study are listed in Table 2.

As expected, Afs35-G20-*AfgapA*^{WT} exhibited the same level of hypoxia fitness as that of Afs35 (Figs. 20B and 20C). Meanwhile, Δ*AfgapA* exhibited the highest hypoxia fitness level among the four investigated strains, strongly indicating that truncation or deletion of AfGapA could be responsible for the developed hypoxia fitness. However, the colony growth of Afs35-G20- *AfgapA*^{WT} and Δ*AfgapA* was impaired similarly to that of their parent strain, Afs35-G20 and Afs35, respectively (Fig. 19A). In addition, similarly to Afs35-G20, Afs35-G20-*AfgapA*^{WT} did not grow at 48 °C, indicating that the remaining *thtA* mutation in this strain is possibly responsible for its reduced thermotolerance.

***AfgapA* dysfunction results in abnormal cellular polarity, poor conidiation and yellowish pigmentation**

In *A. nidulans*, high-level expression of mutant hyperactive RasA in germinating conidiospores results in large, swollen multinucleated cells that do not proceed any further (Som and Kolaparthi 1994; Fillinger et al. 2002), indicating that high Ras activity impairs polarity establishment. Moreover, research involving Ras-GAP in *A. nidulans* also revealed the increment of *gapA* transcript during germination, indicating that *gapA* is directly involved in the polarity establishment (Harispe et al. 2008). This study exhibited similar results for *A. fumigatus*. Abnormally giant swollen conidia (black arrows in Fig. 20) were observed in both Afs35-G20 and Δ*AfgapA* during germination. In addition, the hyphal morphology also appeared to be abnormal in the two AfgapA mutant strains under both hypoxic and normoxic conditions (black arrows in Fig. 21), indicating a disturbed polarity maintenance in the hyphae.

Conidiation reduction has also been reported to be one of the main consequences of the hyperactivation of RasA protein in *A. fumigatus* (Fortwendel et al. 2004). To confirm the role of *AfgapA* in the upstream of RasA regulation pathway, I also investigated the conidiation level. Indeed, 90% and 95% conidiation reduction were observed in Afs35-G20 and Δ*AfgapA,* respectively (Fig. 22A). These results strongly indicate that AfGapA is required to downregulate

Ras activity in *A. fumigatus*. In addition, I observed that the two AfGapA mutants produced yellowish pigments, compared to the wild type (Fig. 22B), indicating that AfGapA may participate in the pigmentation regulation of *A. fumigatus*, which has not been previously reported for the Ras proteins in either *A. fumigatus* or other organisms.

***AfgapA* dysfunction contribute to fungal virulence in the silkworm infection model**

Finally, I evaluated the virulence of the strains using the silkworm infection model. Silkworms have been used as an experimental animal model for elucidating the mechanisms of fungal infection in several pathogenic fungi, including identification of virulence related genes in *Candida* species and *Cryptococcus neoformans* (Ramil et al. 2000; Matsumoto and Sekimizu 2019). In this study, Afs35-G20 showed slightly higher virulence level compared to the wild type, although this difference is not statistically significant (p = 0.2) (Fig. 23A). However, this difference became significant (p = 0.02) when the silkworms were infected with a larger dose of conidia, i.e., 1.5×10^6 /silkworm (Fig. 23B). In addition, Afs35-G20-AfGapA^{WT} exhibited less virulent than Afs35 (Fig. 23A). Moreover, the strain with the complete knockout of *AfgapA*, i.e., Δ*AfgapA,* exhibited the highest virulence level among the investigated strains (Fig. 23A). Consistent with the previous study (Kowalski et al. 2016), the virulence level is highly correlated to their hypoxia fitness.

Based on these and the above data, I conclude that the mutation occurring in Afs35-G20 is a partial loss-of-function mutation, and the truncation or deletion of AfGapA may cause the elongated activation time of Ras protein(s) in *A. fumigatu*s, and is likely to be responsible for the hypoxia adaptation and other observed phenotypic changes.

Discussion

Aspergillus fumigatus plays an important role in the pathogenesis of aspergillosis, and its high rate of mortality is emboldened by its ability to survive and thrive in hypoxic conditions. To reach clinical singularity for this situation, it is important to understand the mechanism of hypoxia adaptation of *A. fumigatus* and the relationship to its pathogenesis. Toward this goal, this study performed a laboratory passaging experiment to generate the adapted strains to hypoxic conditions. Both in vitro and in vivo laboratory passaging experiments have been proven to be insightful in studies of other pathogenic fungi, such as *C. glabrata* and *C. neoformans*. (Franzot et al. 1998; Brunke et al. 2014; Wartenberg et al. 2014). *A. fumigatus* clinical and environmental strains exhibited a great heterogeneity in terms of hypoxia fitness (Kowalski et al. 2016). When investigating the mechanisms of hypoxia adaptation in *A. fumigatus,* it is conceivable that utilizing multiple strains with different genetic backgrounds and hypoxic stress tolerance would greatly enhance these efforts. Thus, the experiments were conducted using multiple strains that have different hypoxic stress tolerance in plate culture. Among the investigated strains, Afs35-G20 was consequently generated, which was confirmed to have increased hypoxia fitness in liquid culture when compared to the parental strain.

With the application of whole genome sequencing, a resultant mutation was identified in *AfgapA* (Afu3g09900)*,* which encodes the Ras-GAP protein in *A. fumigatus*. AfGapA is highly conserved among fungi, including the filamentous fungi *A. nidulans*, *S. pombe* and *S. cerevisiae*. According to BLASTP results, there are no other *AfgapA* paralogs in *A. fumigatus*. To investigate the physiological functions of this Ras-GAP, which is, AfGapA, I constructed the reconstituted strain of Afs35-G20 harboring a wild type *AfgapA* allele, as well as a *AfgapA* null mutant, to observe and compare the phenotypic changes against the wild type. As expected, the reconstitution of wild type AfGapA in Afs35-G20 caused a recovery of low hypoxia fitness. Furthermore, the null mutant of AfGapA exhibited more severe phenotypes compared to Afs35-G20, like higher hypoxia fitness, virulence, and reduced conidiation level. In addition, a yellowish pigmentation in both Afs35-G20 and Δ*AfgapA* was also observed. These results indicate that the truncation and/or deletion of AfGapA is required for the hypoxia fitness, virulence, and conidia pigmentation in *A. fumigatus*.

Ras proteins are members of a family of small monomeric GTPases that are highly conserved in fungal kingdom. Ras and Rho subfamilies regulate actin rearrangements (Hall 1998). Ras activity is controlled by guanosine nucleotide diphosphate (GDP)/guanosine nucleotide triphosphate (GTP) binding via a binary switch fashion. Two factors regulate Ras, namely guanine nucleotide exchange factors (GEFs) and GTPase-activating proteins (GAPs) (Fig. 16). Ras-GAP regulates a variety of morphogenetic processes by deactivating its substrate protein Ras (Som and Kolaparthi 1994; Harispe et al. 2008; Norton and Fortwendel 2014), whereas GEFs exchange Ras-

bound GDP with GTP. Although it has been reported that Ras proteins in *A. fumigatus* are important regulators of hyphal morphogenesis and virulence (Fortwendel et al. 2004; Norton and Fortwendel 2014), this study reports the function of one of its upstream regulator, Ras-GAP (*AfgapA*), for the first time.

Increased hypoxia fitness in both Afs35-G20 and Δ*AfgapA* was observed, compared to the parental strain, Afs35 (Figs. 20B and 20C). Specifically, the fungal biomass of Afs35-G20 and Δ*AfgapA* were higher than that of Afs35 in hypoxia, whereas those were comparable to that of Afs35 in normoxia (Fig. 19B). The hyphal morphologies of Afs35, Afs35-G20 and Δ*AfgapA* were similar under both hypoxic and normoxic conditions (Fig. 21). Thus, the increased fungal biomass of Afs35-G20 and Δ*AfgapA* in hypoxia may be due to their higher germination rates, suggesting that *AfgapA* may function in the germination, particularly in hypoxia. *A. fumigatus* has two Ras homologues, i.e., RasA and RasB, which play important roles in cellular processes and pathogenesis (Fortwendel et al. 2004; Norton and Fortwendel 2014). It has been reported that the deletion of either RasA or RasB results in reduced virulence (Fortwendel et al. 2005) due to the overlapping functions of the two homologues. Thus, since RasA and/or RasB could be the targets of *AfgapA*, investigating the Ras specificity of *AfgapA* would be an intriguing topic for future studies.

Strains harboring constitutively active Ras reportedly exhibit highly branched hyphae, reduced conidiation, and increased virulence in *A. fumigatus* (Fortwendel et al. 2004, 2009, 2012). In *A. nidulans*, Ras-GAP encoding gene GapA is essential for the polarity establishment and maintenance (Harispe et al. 2008). Microscopic observation of strains carrying the *gapA* mutation showed that a proportion of germinating conidia do not give rise to a germ tube but continue growing isotopically while nuclei undergo mitosis, yielding giant, multinucleate spherical cells, suggesting that polarity establishment is affected by this mutation. *gapA*Δ also showed abnormally swollen regions and apical branching. Consistent with this, abnormally giant conidia during germination (Fig. 20), abnormally swollen regions and apical branching in the hyphae were observed in Afs35-G20 and Δ*AfgapA* (Fig. 21). Taken together, these observations strongly supported the hypothesis that *AfgapA* dysfunction downregulates its substrate Ras protein, followed by hyperactivation of Ras.

In addition to higher hypoxia fitness and virulence, Afs35-G20 and Δ*AfgapA* also produced a yellowish pigmentation in the conidia (Fig. 22B). This was consistent with a previous study showing that the main pigment ingredient in conidia (melanin) plays a protective role against environmental conditions and in pathogenicity (Brakhage and Liebmann 2005). The outer layer of the conidia is composed of a hydrophobic polymer, dihydroxynaphthalene (DHN) melanin, which protects *A. fumigatus* against host defense. Genes in the melanin cluster have been proved to be necessary for the structure and stiffness maintenance of the conidial cell wall, and

consequently, the virulence (Latgé et al. 2017). In terms of the pigmentation regulation in *A. fumigatus*, *wetA* participates in the conidial pigmentation pathway by downregulating the expression of *wA*, which encodes a polyketide synthase (PKS) necessary for the formation of a key conidial pigment (Mayorga and Timberlake 1992). Meanwhile, the expression of *rasA* was upregulated in Δ*wetA* in *A. fumigatus*, indicating that *rasA* may participate in the pigmentation pathway by downregulating *wetA* (Wu et al. 2018). Thus, the yellowish pigmentation occurred in AfGapA mutants may be caused by the hyperactivation of RasA, indicating that *AfgapA* may suppress the pigmentation during conidiogenesis.

The Ras homolog in *C. neoformans*, Ras1, has been proved to be necessary for the hypoxia adaptation (Chang et al. 2014). However, the role of Ras in hypoxia adaptation in *A. fumigatus* yet. In this study, acquirement of hypoxia fitness in the two AfGapA mutant strains indicate a similar role of Ras in hypoxia responses of Ras protein(s) of *A. fumigatus*. Various mechanisms of oxygen sensing and responses to hypoxia in yeast and pathogenic fungi have been reviewed recently (Willger et al. 2008). The mammalian sterol regulatory element-binding protein (SREBP) is an important factor controlling oxygen sensing and virulence in *A. fumigatus* and other pathogenic fungi. Its homolog SrbA in *A. fumigatus* also controls proper cell polarity. Additionally, the null mutant of SrbA also displayed increased susceptibility to the azole class of antifungal drugs (Willger et al. 2008), although the mechanism behind this result is currently unknown. However, the deletion of AfGapA does not change the antifungal susceptibility level (Table 3), suggesting different pathways from SrbA regulated hypoxia responses.

In summary, the Ras-GAP protein AfGapA in *A. fumigatus* shares a striking similarity with that of other closely related yeasts or pathogenic fungi, in terms of a broad range of physiological functions, including regulating the conidiation, pigmentation, hypoxia fitness, and virulence. Taken together, this study contributes to the understanding of AfGapA-regulated Ras activity in *A. fumigatus*. More importantly, this study indicates that ΔAfGapA causes developed hypoxia fitness, which is also confirmed to be crucial for the virulence of *A. fumigatus*. The strong downregulation of fungus-specific participants in Ras protein activation and signaling could be a promising focus for the future development of novel antifungal treatments. However, because of the complexity of the Ras regulated pathways, further studies are required to elucidate the role of AfGapA in the Ras-mediated pathways and its involvement in the hypoxia adaptation and pathogenicity.

Figures and tables

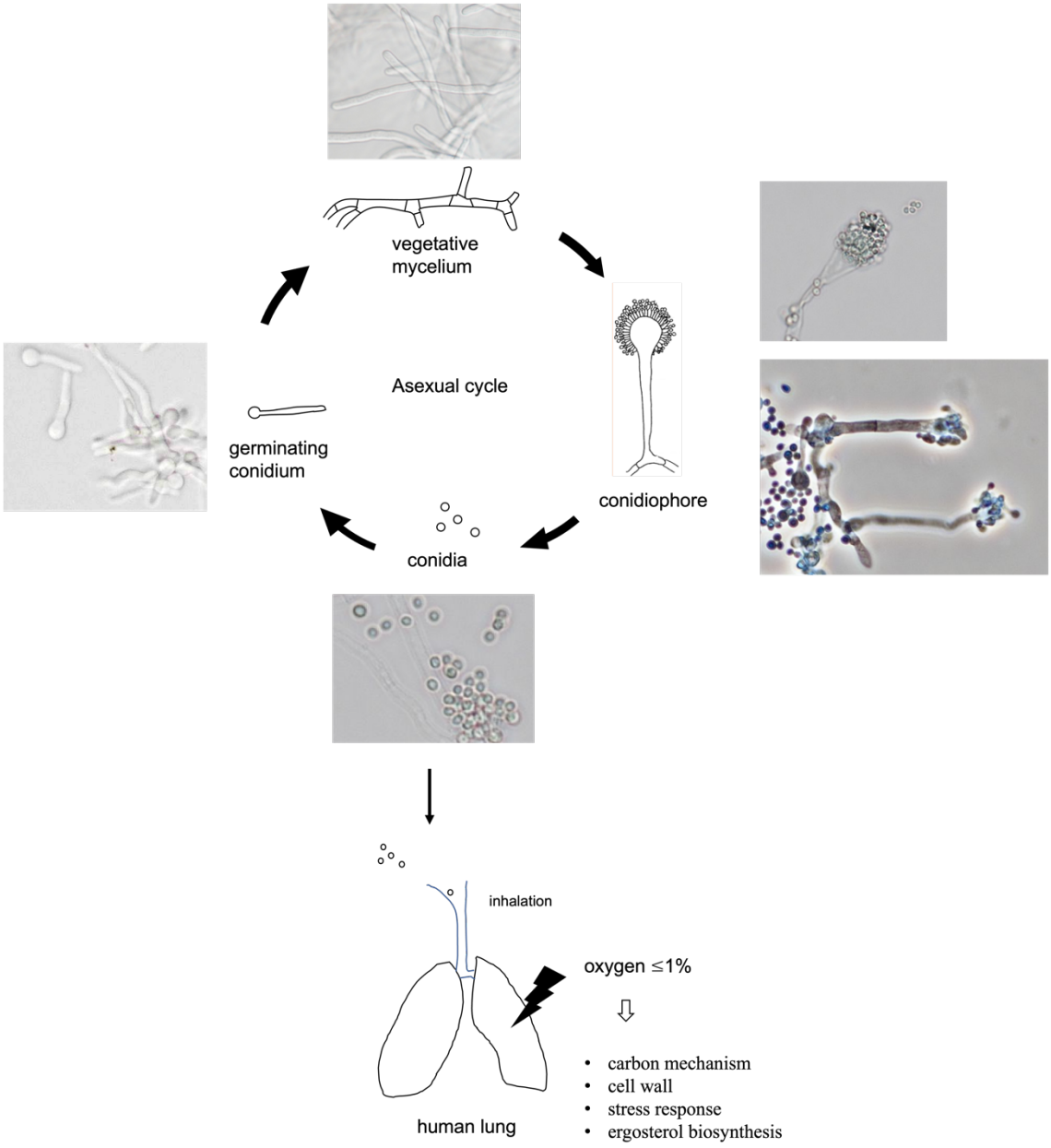

Fig. 1 *A. fumigatus* conidia is exposed to the hypoxic microenvironment in human lungs. Oxygen availability is supposed to be less than 1% in the infection site (Wezensky and Cramer 2011). Hypoxia influences various metabolic process in both fungi and the host.

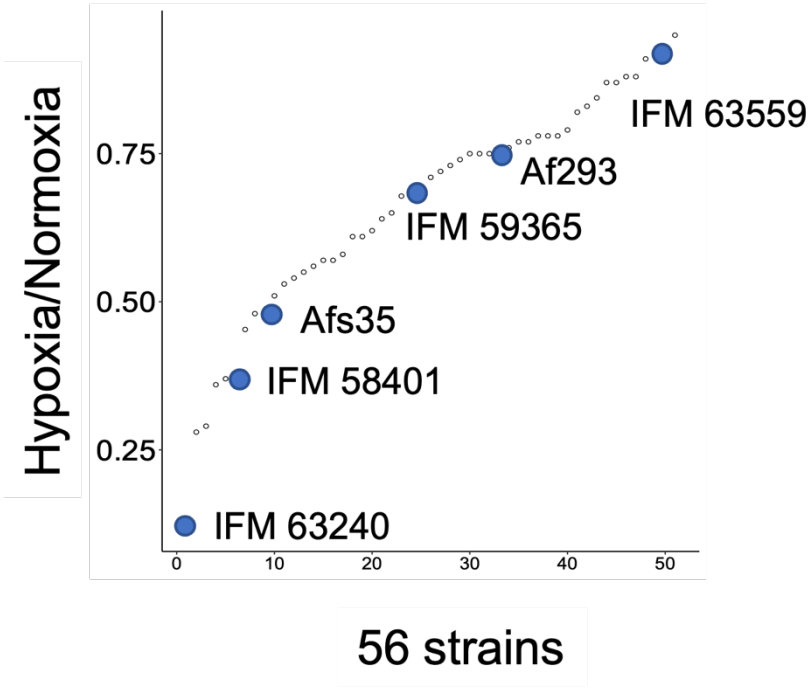

Fig. 2 Hypoxia fitness in colony growth of 56 *A. fumigatus* clinical strains. A total of 1×10^3 conidia were inoculated in GMM, and cultured for four days, 37 °C under hypoxic and normoxic conditions, respectively. Diameters of colony growth were afterwards measured, and the ratio of diameter in hypoxia and that in normoxia was calculated for each strain. Six strains that were selected for the following laboratory passaging experiment are colored blue.

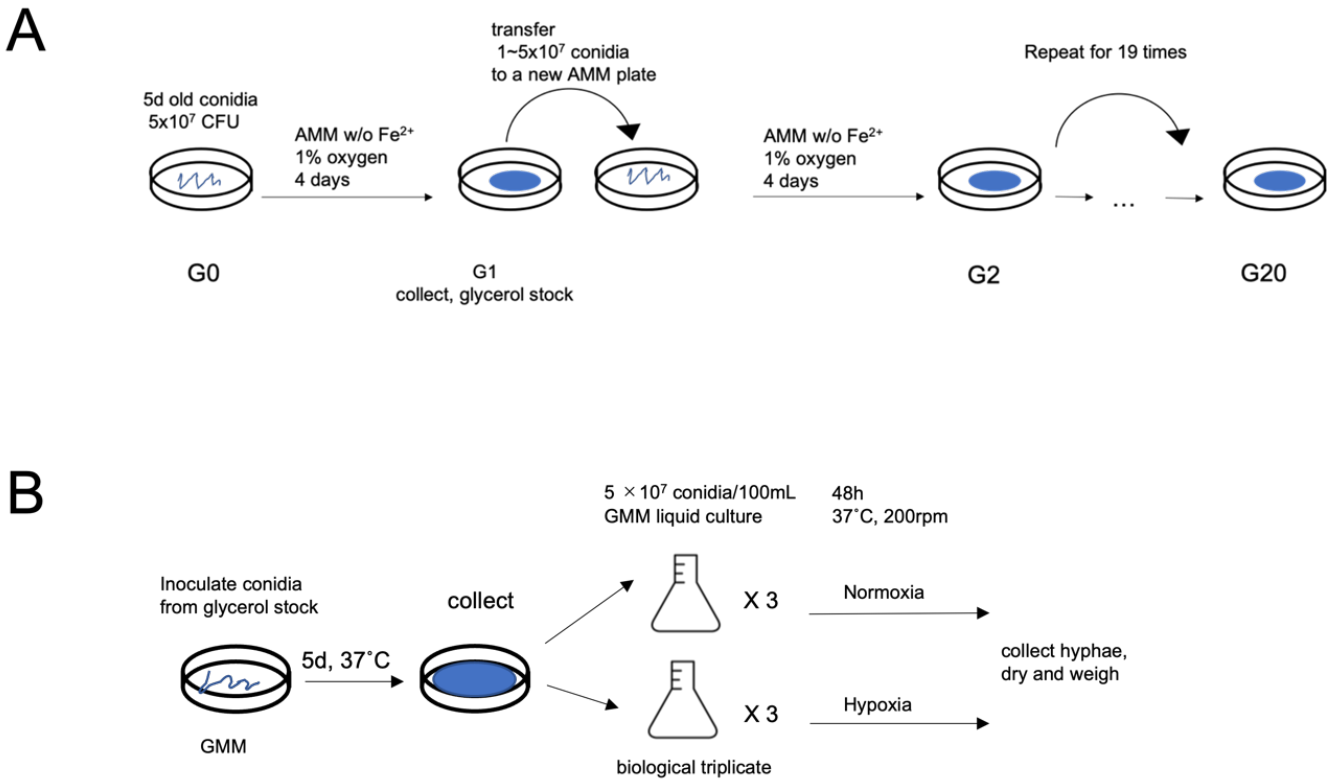

Fig. 3 Schematic diagrams of the experimental procedure. (A) Laboratory passaging experiment. (B) Fungal biomass measurement. A total of 5×10^7 conidia were inoculated in 100 mL GMM and cultured for 48h, 37 °C, shaking at 200 rpm under hypoxic and normoxic conditions. Biomass tissue was then collected, dried, and weighed.

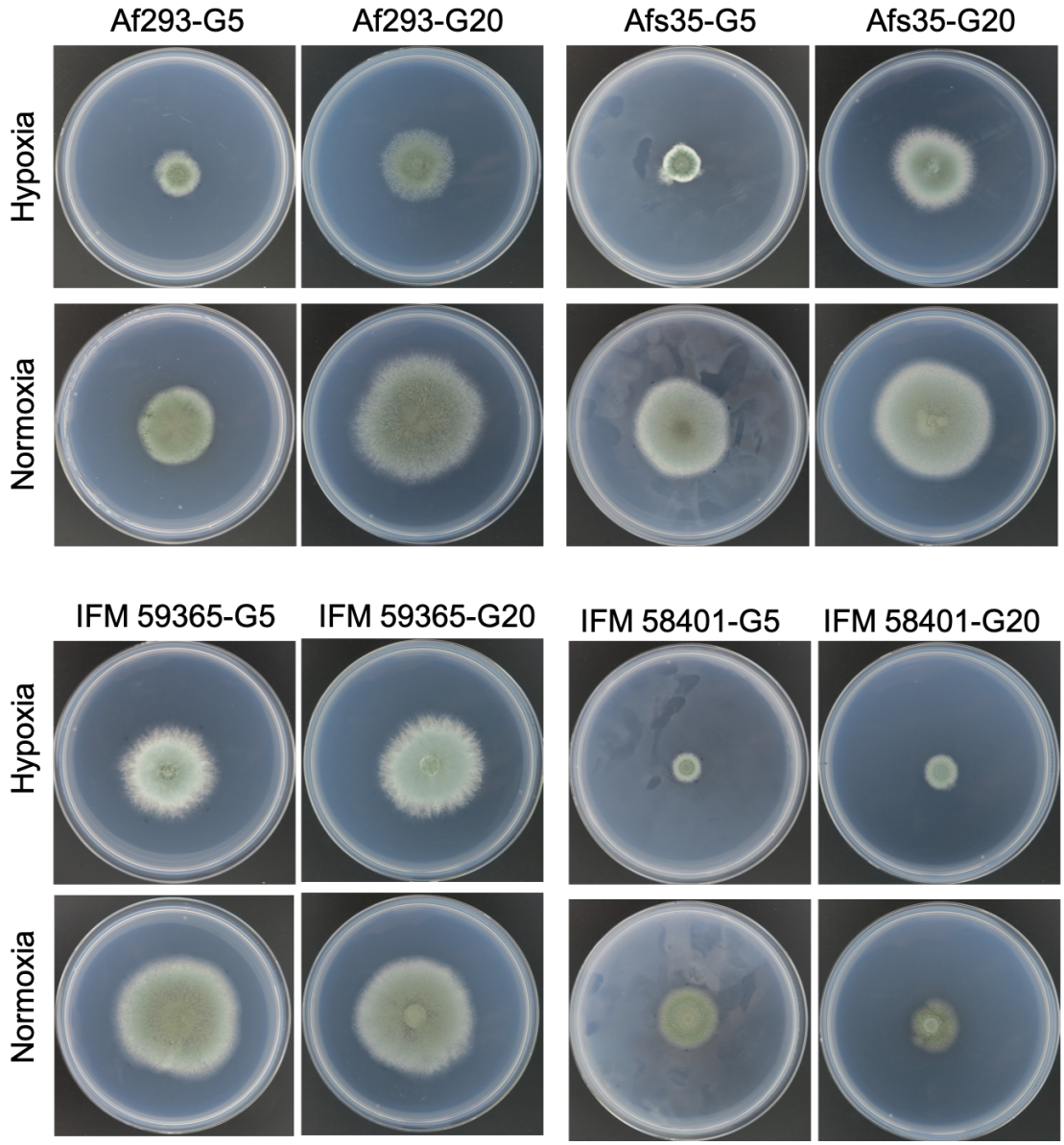

Fig. 4 Colony growth characterization of G5 and G20 of four investigated strains in hypoxia and normoxia. A total of 1×10^3 conidia for each strain were inoculated and grown on GMM, 37 °C for four days.

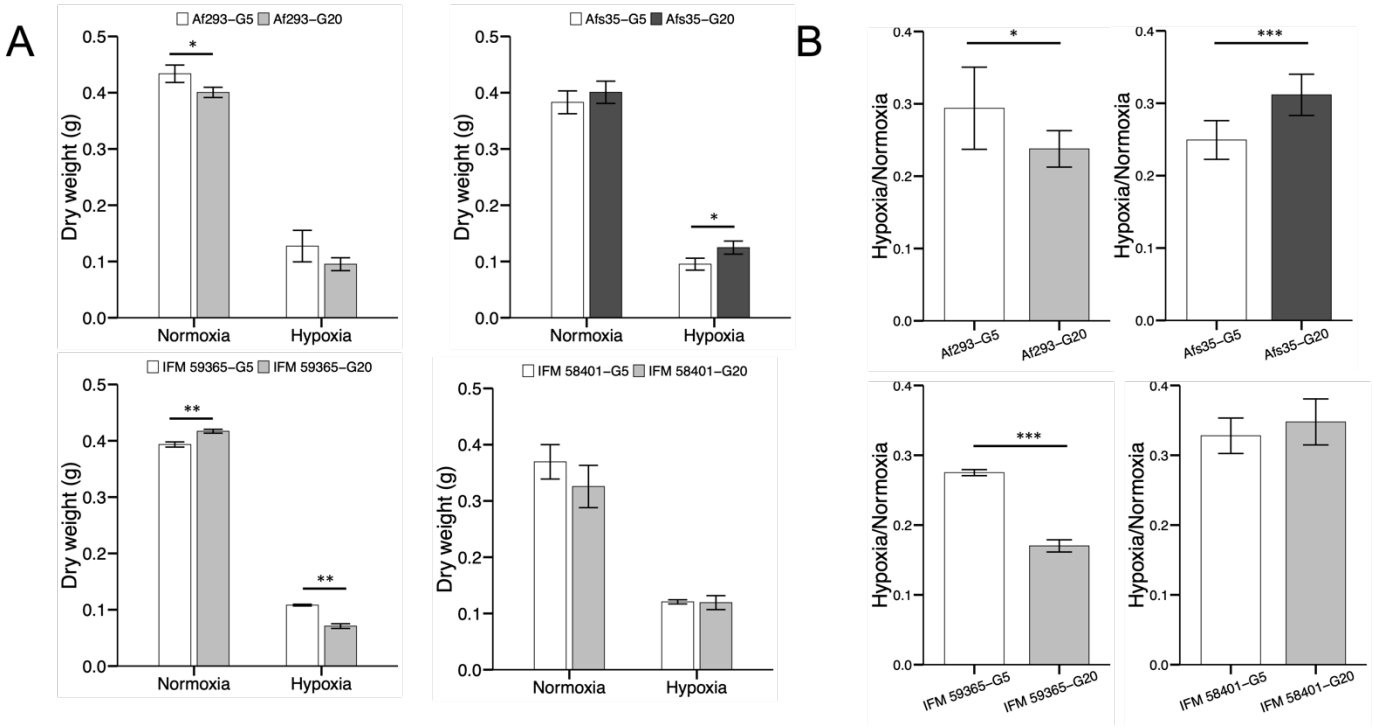

Fig. 5 Biomass production in liquid culture of G5 and G20 of four investigated strains in hypoxia and normoxia. Afs35-G20 was indicated with deep grey. (A) Dry weight. A total of 5×10^7 conidia were inoculated in 100 mL GMM and cultured for 48h, 37 °C shaking at 200 rpm under hypoxic and normoxic conditions. (B) The ratio of biomass weight in hypoxia to that in normoxia. Statistical analysis was performed using a two-tailed *t*-test (*, *p*-value < 0.05; **, *p*-value < 0.01; ***, *p*-value < 0.001).

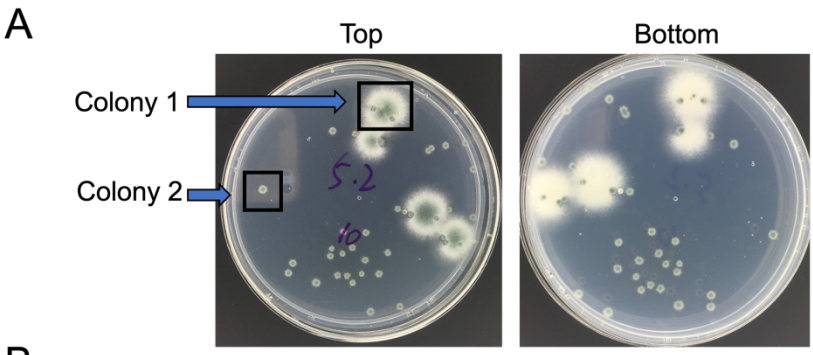

B

	2A	2B	2C	3B	4A	4C
Afs35	n.a.	19	8	9	11	6
Afs35-G20 colony1	14	19	8	9	11	6
Afs35-G20 colony2	14	19	8	9	11	6

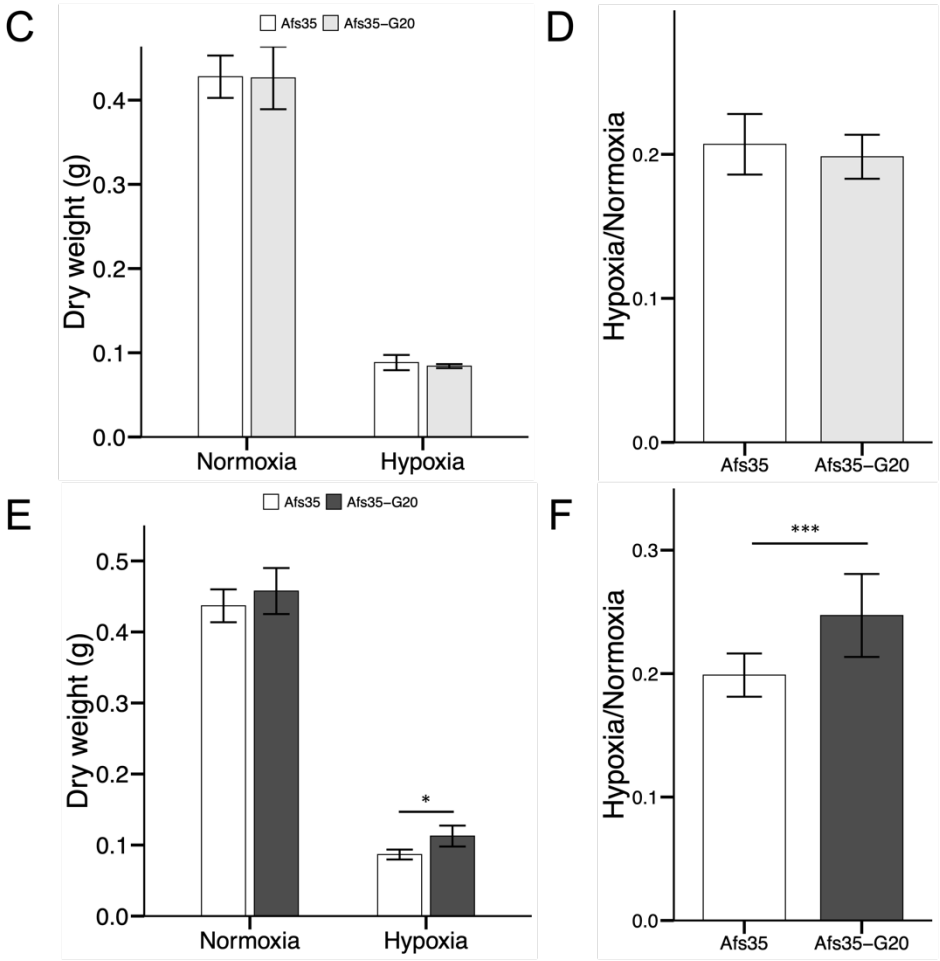

Fig. 6 Single colony isolation of Afs35-G20 and growth phenotypes of the two isolates. (A) Two colonies were observed in Afs35-G20, exhibiting different morphological features. (B) STRs of

(**Fig. 6** continued) the two Afs35-G20 colonies and Afs35. Dry weight of biomass of Afs35 and Afs35-G20 colony 1 (C) and colony 2 (E). H/N biomass ratio of colony 1 (D) and colony 2 (F). A total of 5×10^7 conidia were inoculated in 100 mL GMM and cultured for 48h, 37 °C, shaking at 200 rpm under hypoxic and normoxic conditions. Statistical analysis was performed using a two-tailed *t*-test (*, *p*-value < 0.05; ***, *p*-value < 0.001).

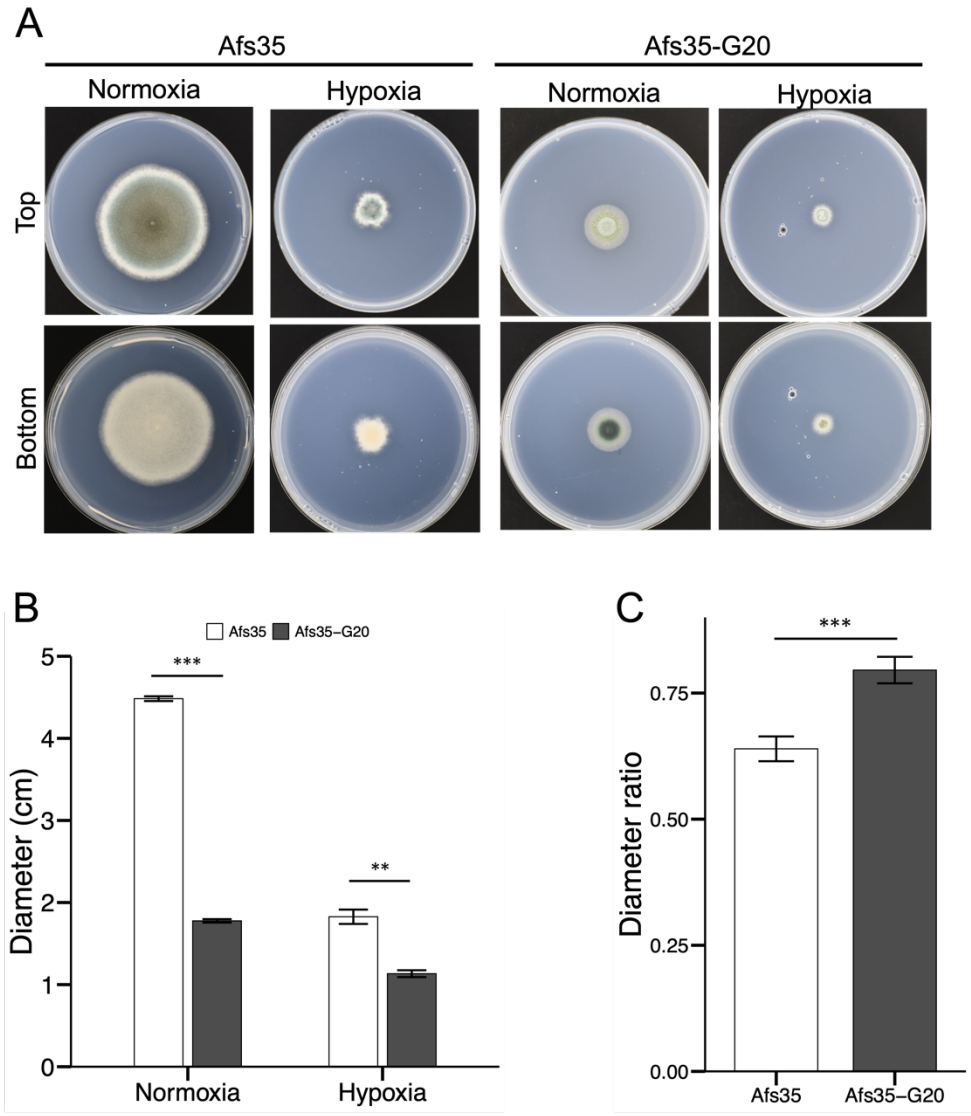

Fig. 7 Growth phenotypes of Afs35 and Afs35-G20. (A) Growth assays. (B) Colony diameters under hypoxic and normoxia conditions were measured. (C) H/N diameter ratios were calculated. A total of 1×10^3 conidia for each strain were inoculated and grown on GMM, 37 °C for four days. Statistical analysis was performed using a two-tailed *t*-test (**, *p*-value < 0.01; ***, *p*-value < 0.001).

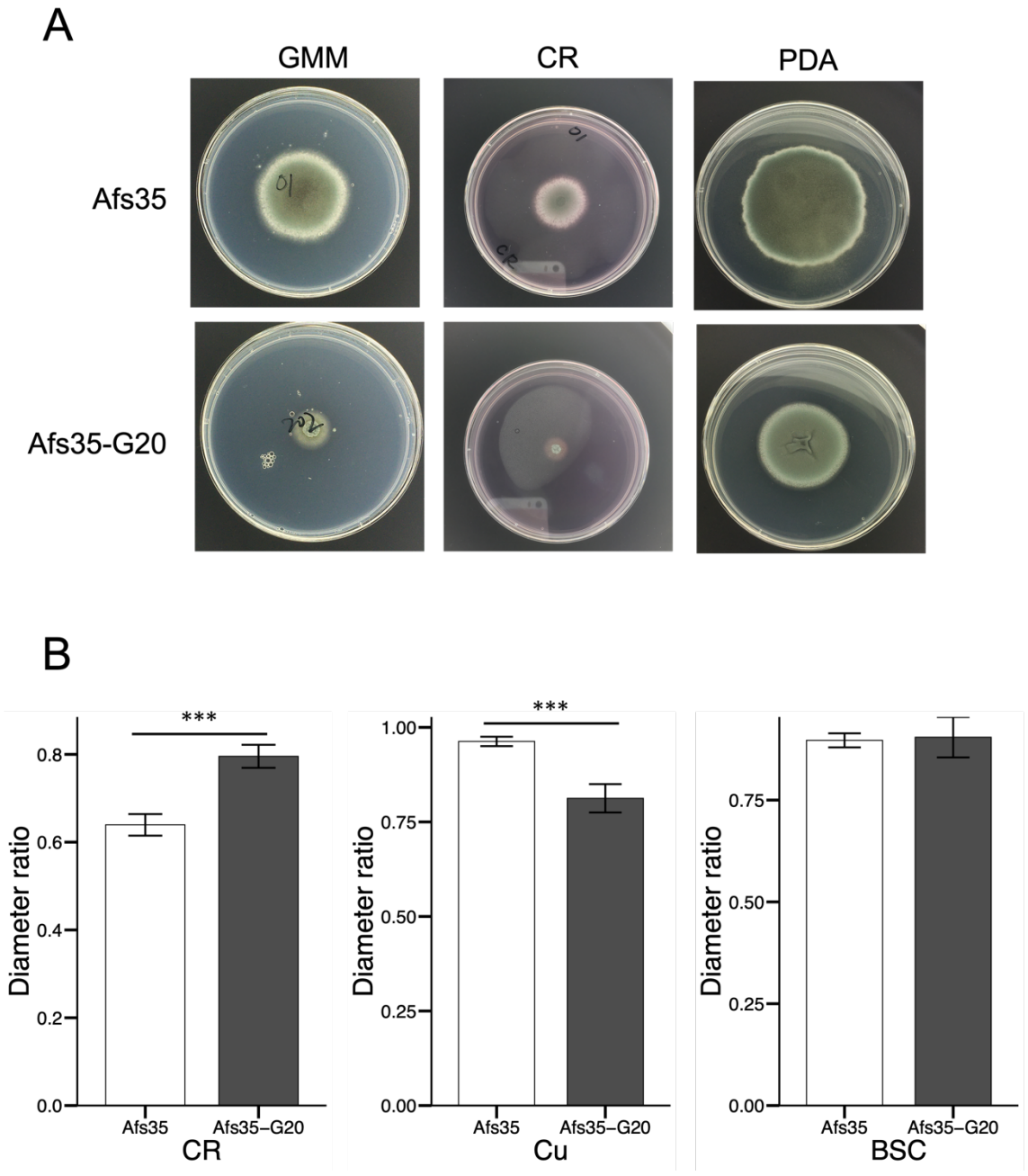

Fig. 8 Growth assays in CR, copper, and BSC. (A) Growth phenotypes of Afs35 and Afs35-G20 in GMM, GMM containing 10 μg/ml CR, and PDA medium. (B) The ratio of colony diameter in GMM containing the respective reagent, and that in plain GMM. Statistical analysis was performed using a two-tailed *t*-test (***, *p*-value < 0.001).

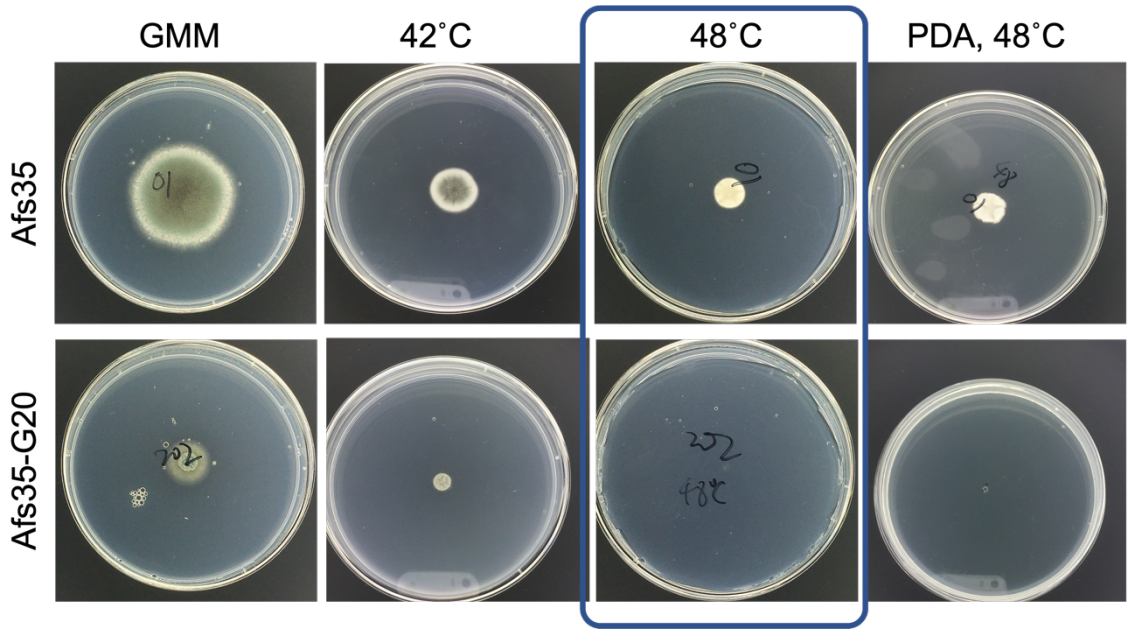

Fig. 9 Thermotolerance testing of Afs35 and Afs35-G20. A total of 1×10^3 conidia for each strain were inoculated and grown for four days.

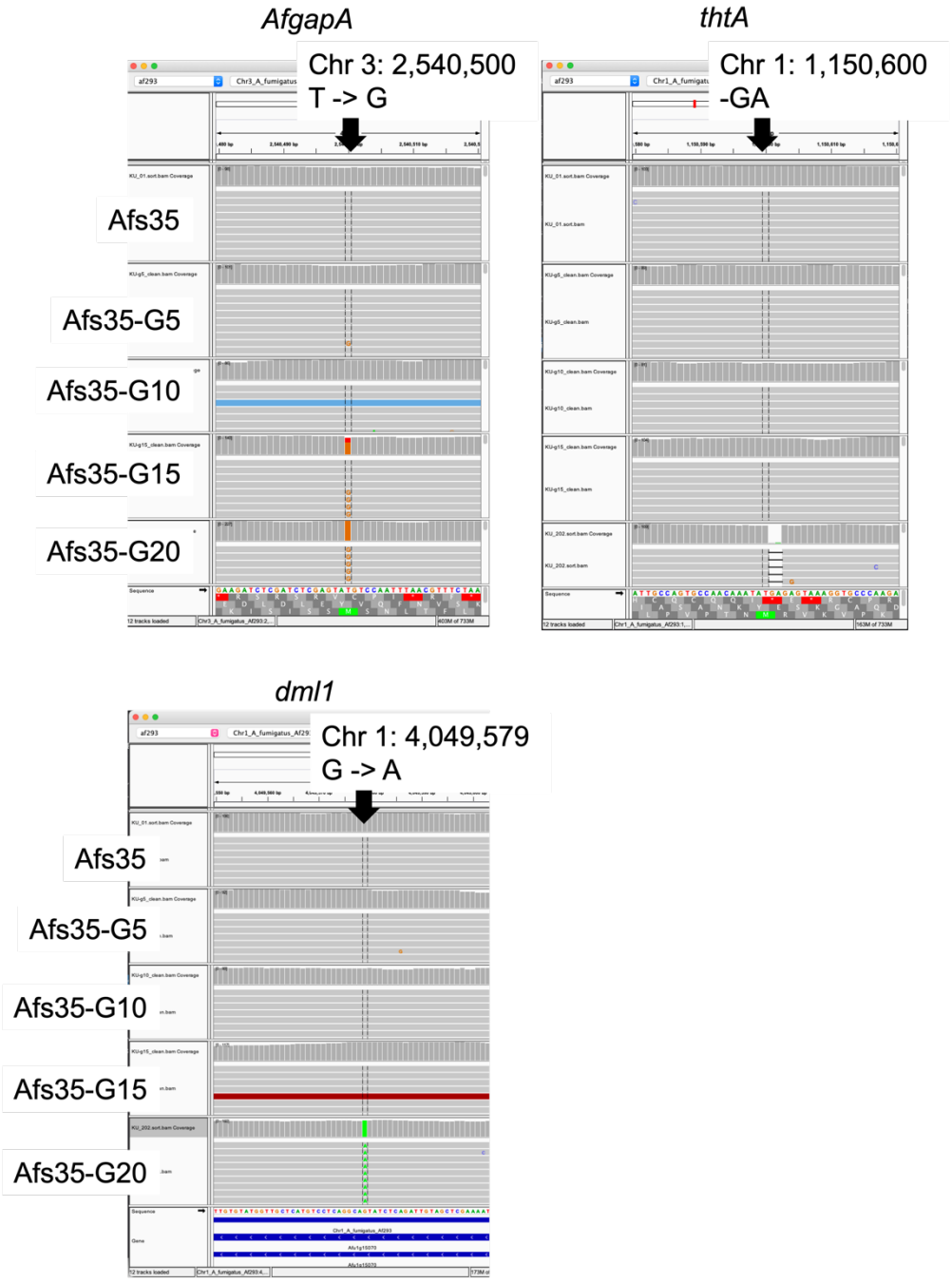

Fig. 10 Snapshots of the mapping results of Afs35 and Afs35's G5, G10, G15, and G20. Two missense mutations in *AfgapA* and *thtA*, and a synonymous mutation in *dml1* are presented. The point mutations are indicated by black arrows.

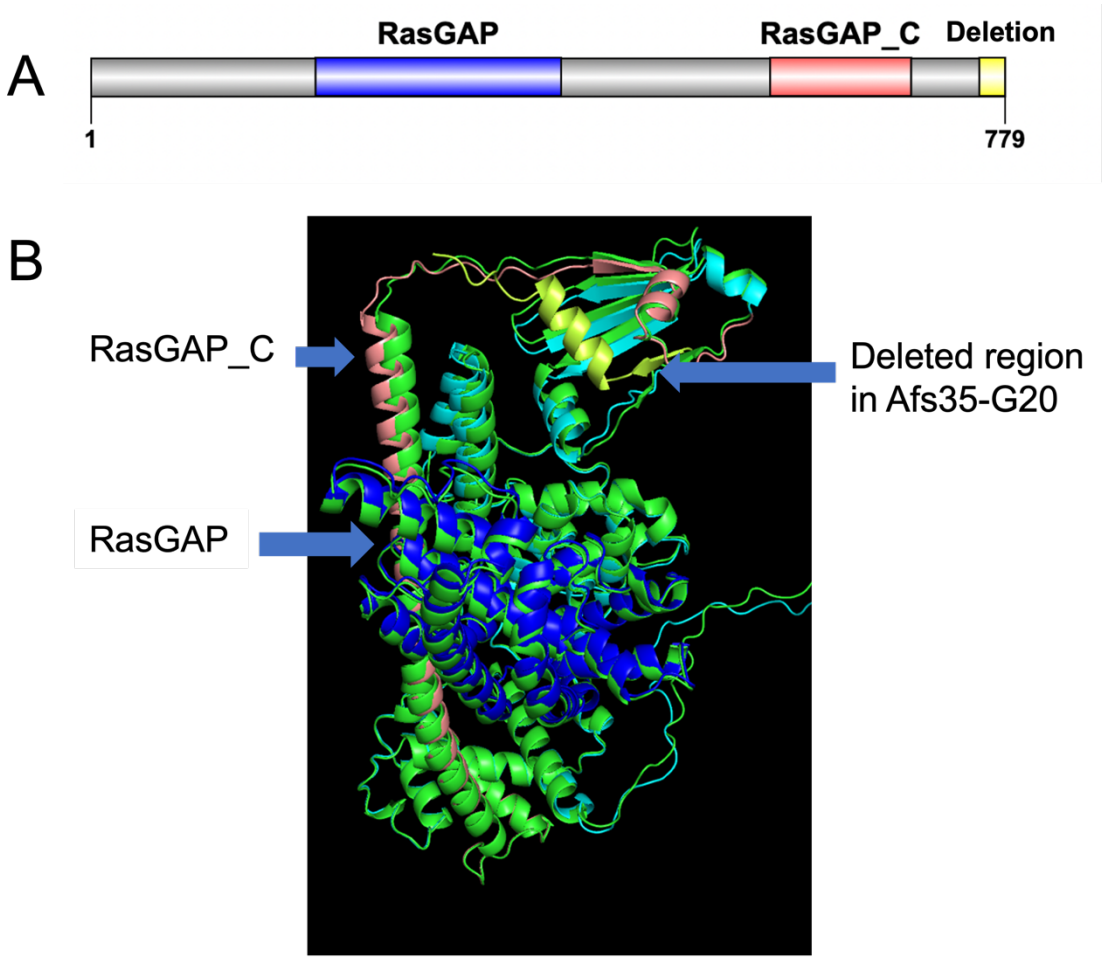

Fig. 11 Protein structures of AfGapA and AfGapA^{Tyr757Ter}. (A) Secondary structure of AfGapA. AfGapA harbors “Ras-GAP” (PF00616) and “Ras-GAP_C” (PF03836) domains. (B) Tertiary structures of AfGapA and AfGapA^{Tyr757Ter}.

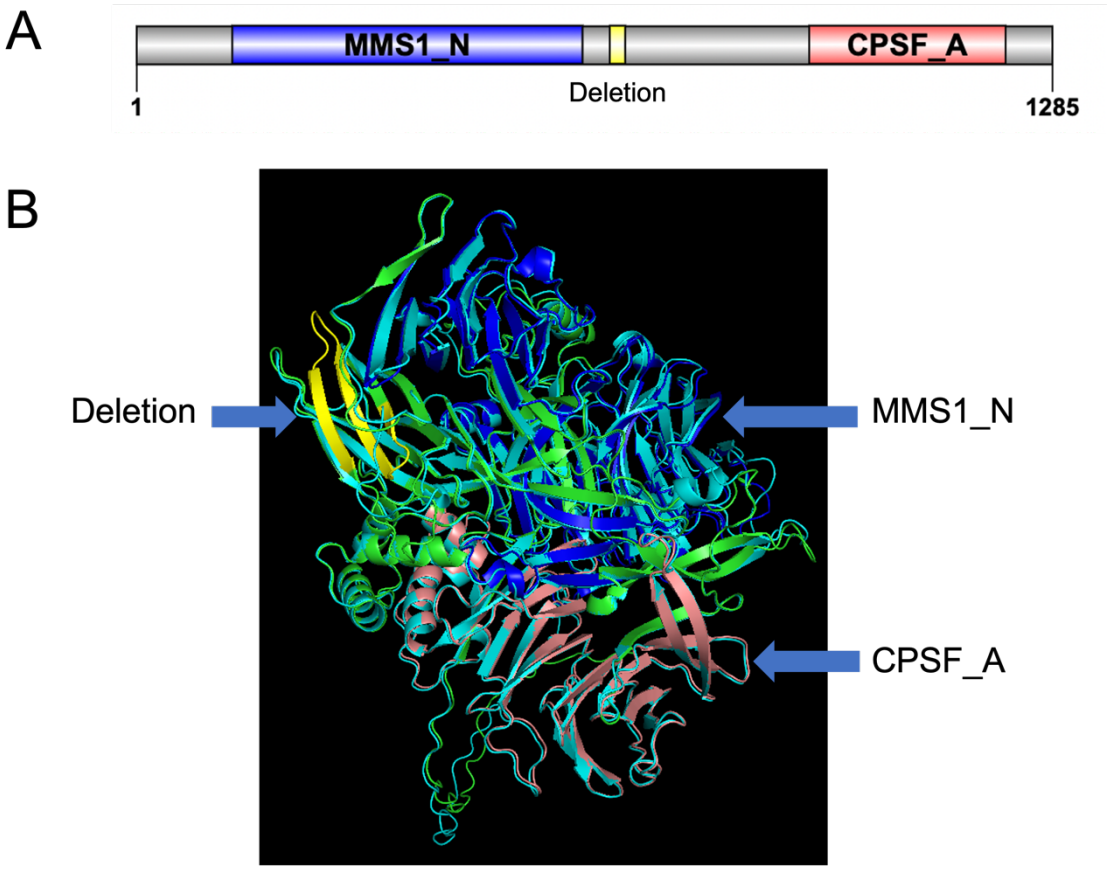

Fig. 12 Protein structures of THTA and THTA^{mut}. (A) Secondary structure of THTA. THTA harbors "MMS1_N" (PF10433) and "CPSF_A" (PF03178) domains. (B) Tertiary structures of THTA and THTA^{mut}.

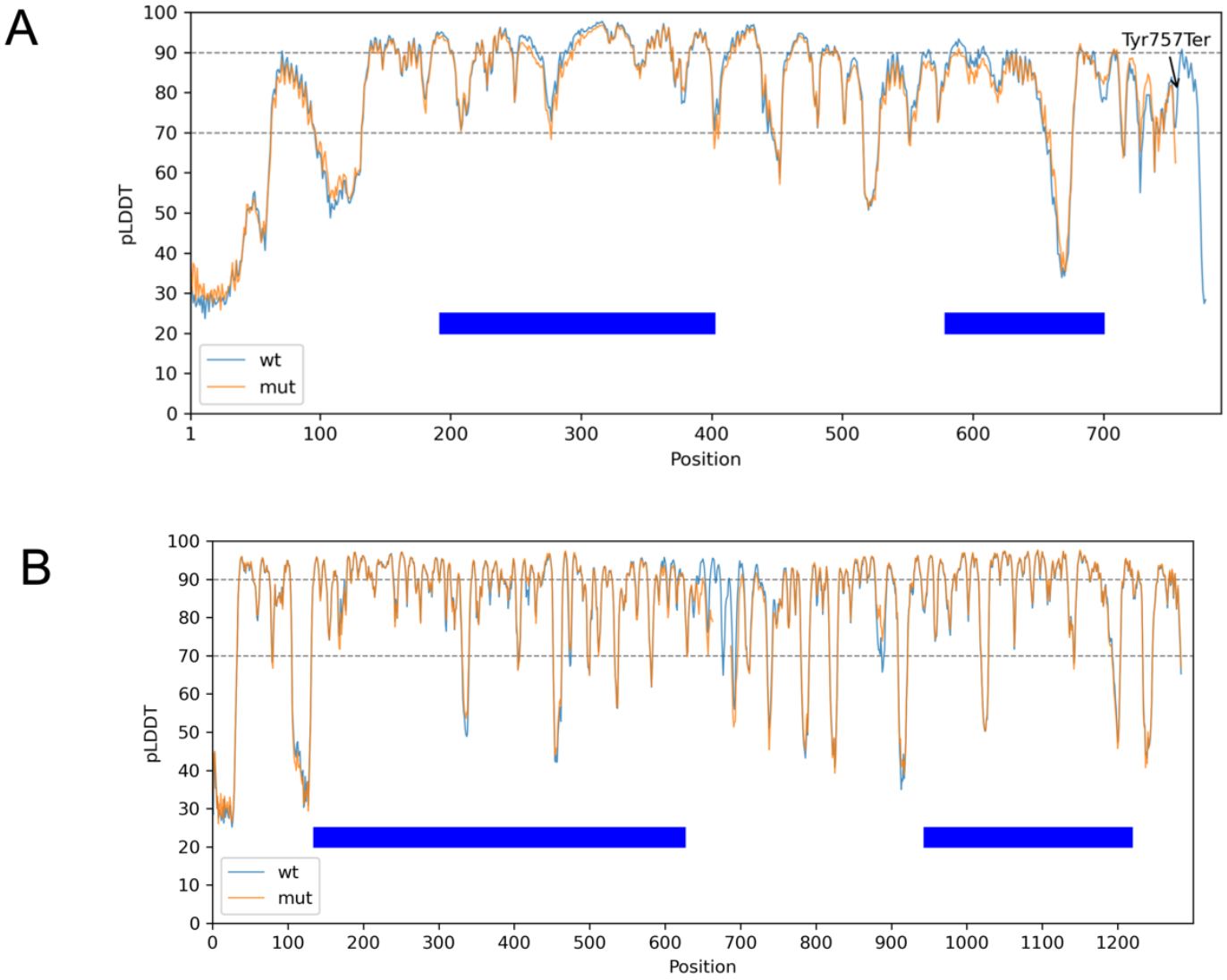

Fig. 13 pLDDT scores derived from the AlphaFold2 structures. (A) AfGapA (blue) and AfGapA^{Tyr757Ter} (yellow). Mean values of pLDDT score are 79.2 and 79.1, respectively. (B) THTA (blue) and THTA^{mut} (yellow). Mean values of pLDDT score are 83.3 and 83.2, respectively. Blue bars indicate protein domains.

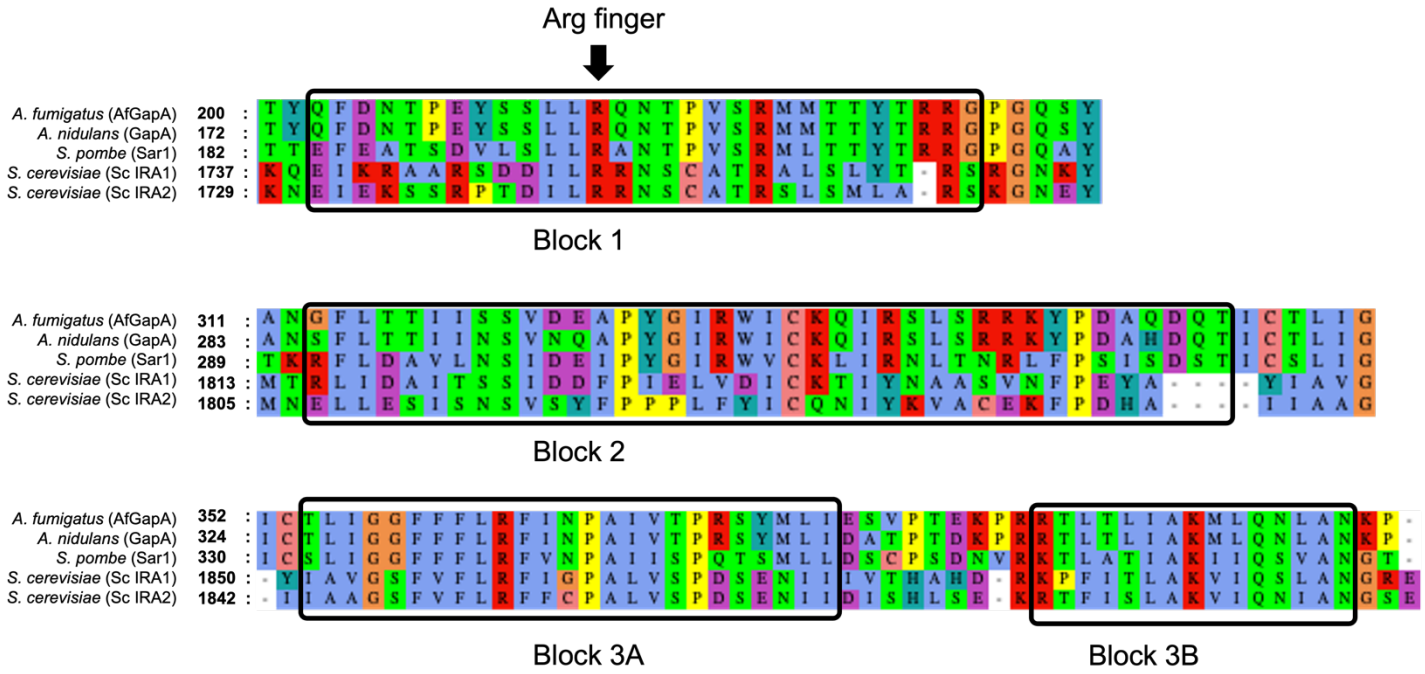

Fig. 14 Multiple alignment of four characteristic amino acid blocks of Ras GAPs in *A. fumigatus, A. nidulans, S.cerevisiae,* and *S. pombe*. Black arrow indicates Arg finger.

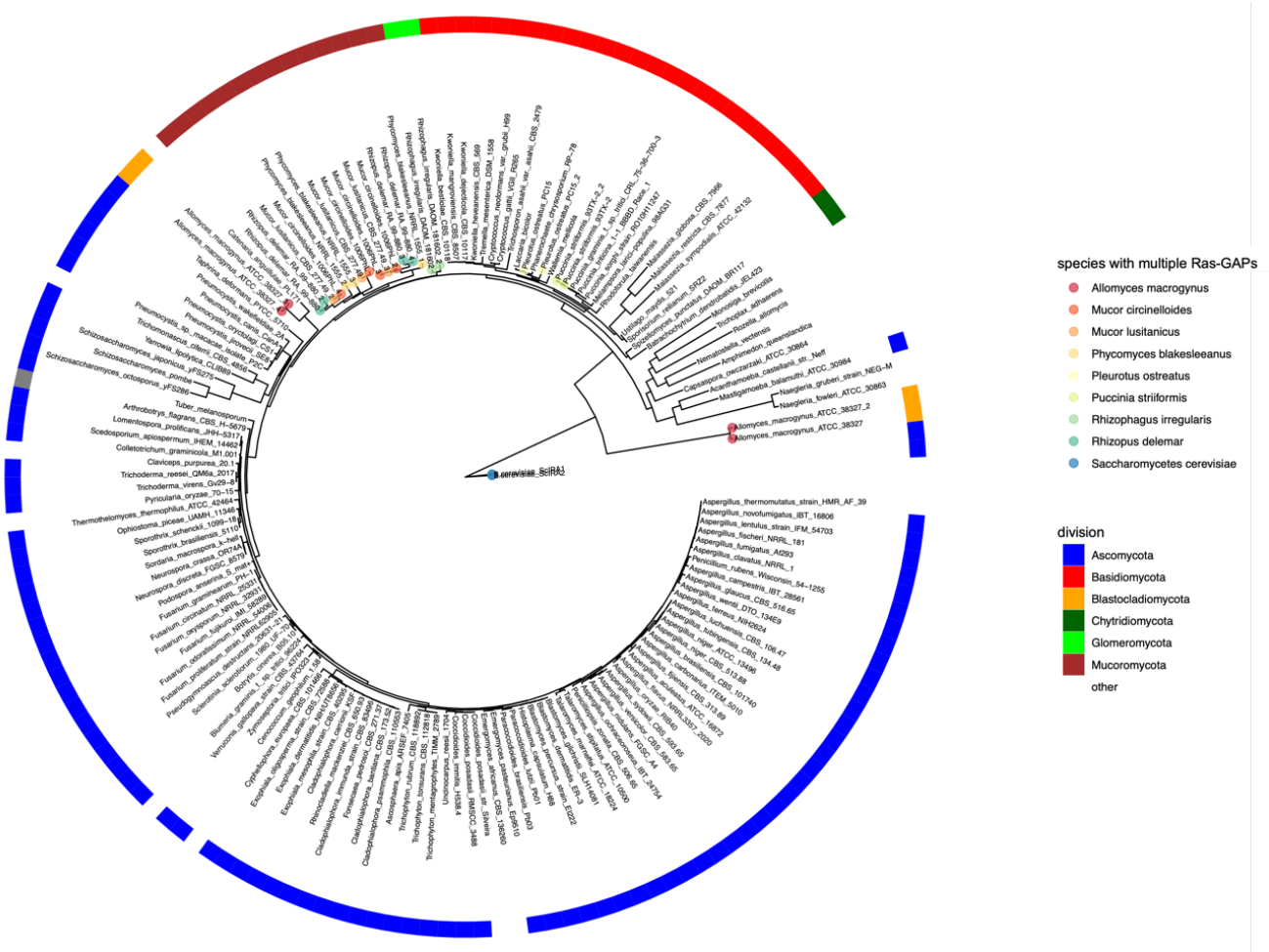

Fig. 15 Phylogenetic tree based on 155 amino acid sequences among Ascomycota, Basidiomycota, etc. Species with multiple Ras-GAPs are indicated with color circles.

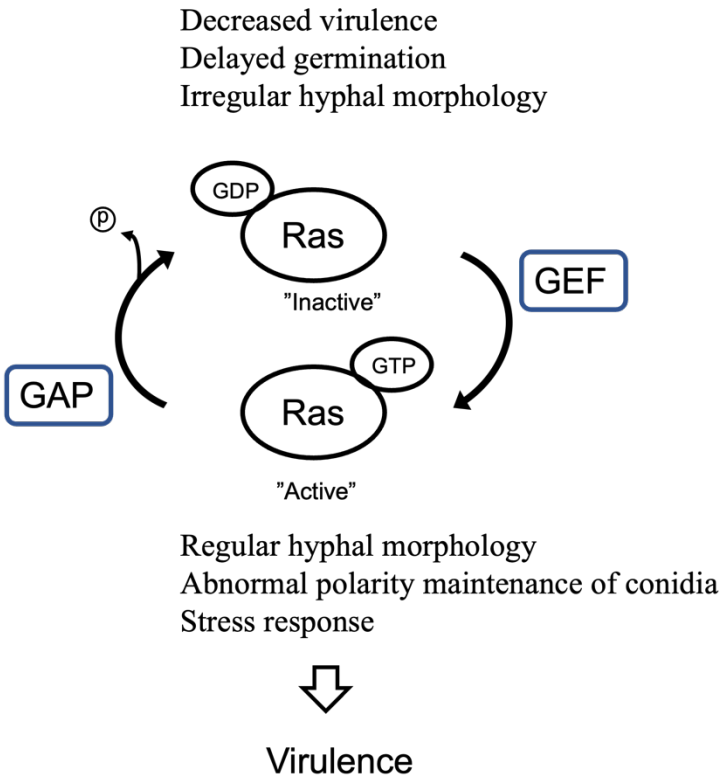

Fig. 16 Model representing the RasA activity in *A. fumigatus* and other fungi. GEF, guanine exchange factor; GAP, GTPase-activating protein.

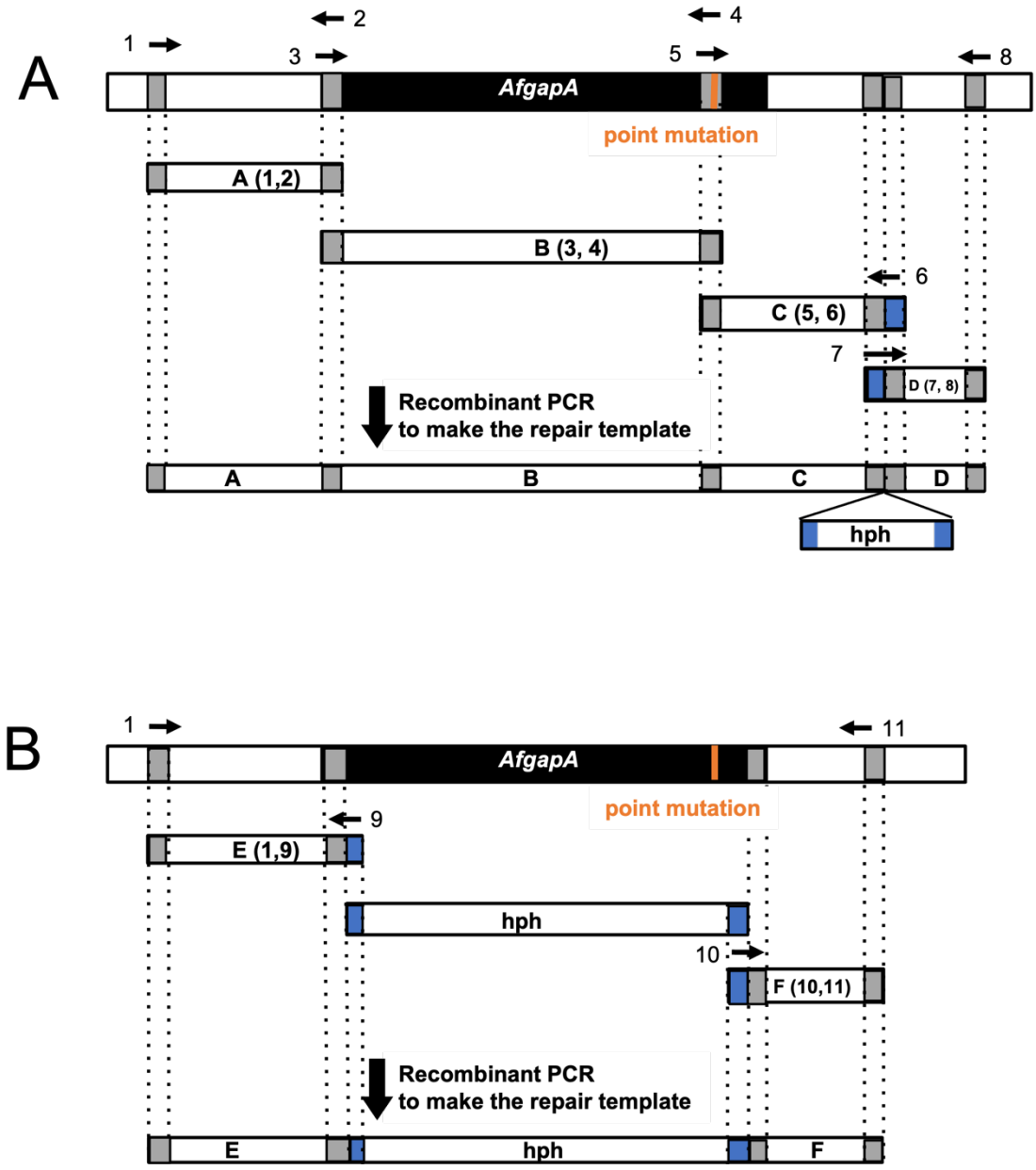

Fig. 17 Schematic diagram for construction of (A) Afs35-G20-*AfgapA*^{WT} and (B) Δ*AfgapA*. The *hph* gene was amplified from the pHph plasmid. Primers containing sequences from *hph* were colored with blue. The repair templates were then used for transformation.

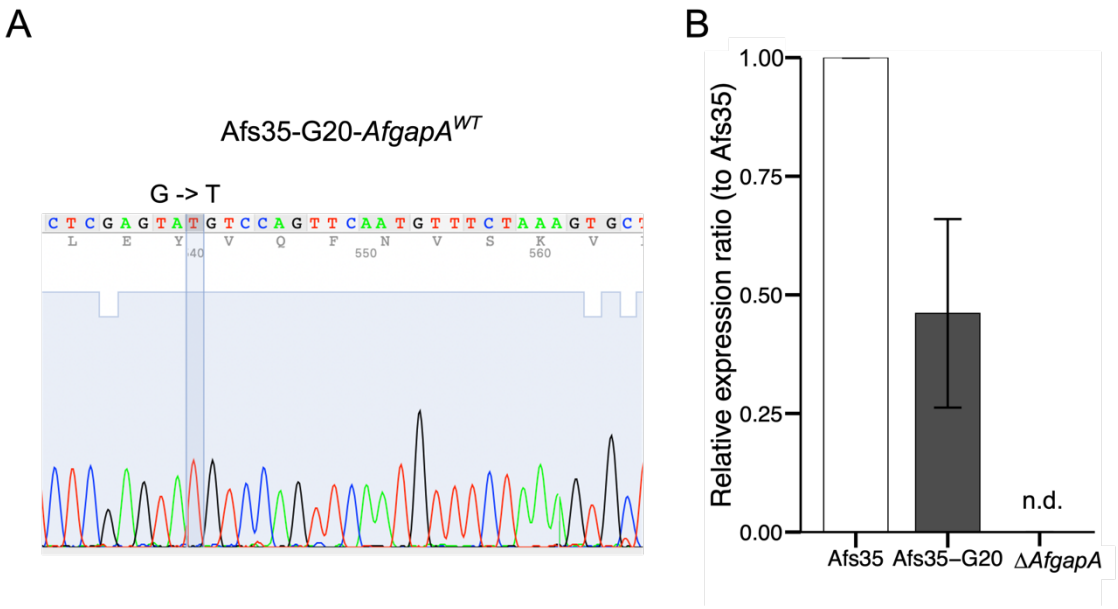

Fig. 18 The confirmation of the successful transformants. (A) The successful replacement from G to T in a Afs35-G20-*AfgapA*^{WT} transformant was confirmed by Sanger sequencing. (B) The successful disruption of *AfgapA* was confirmed by the Quantitative real-time RT-PCR analysis of *AfgapA* in Afs35, Afs35-G20, and Δ*AfgapA*. All relative ratios to Af293 were calculated using the $2^{-\Delta\Delta Ct}$ method. n.d., not detected

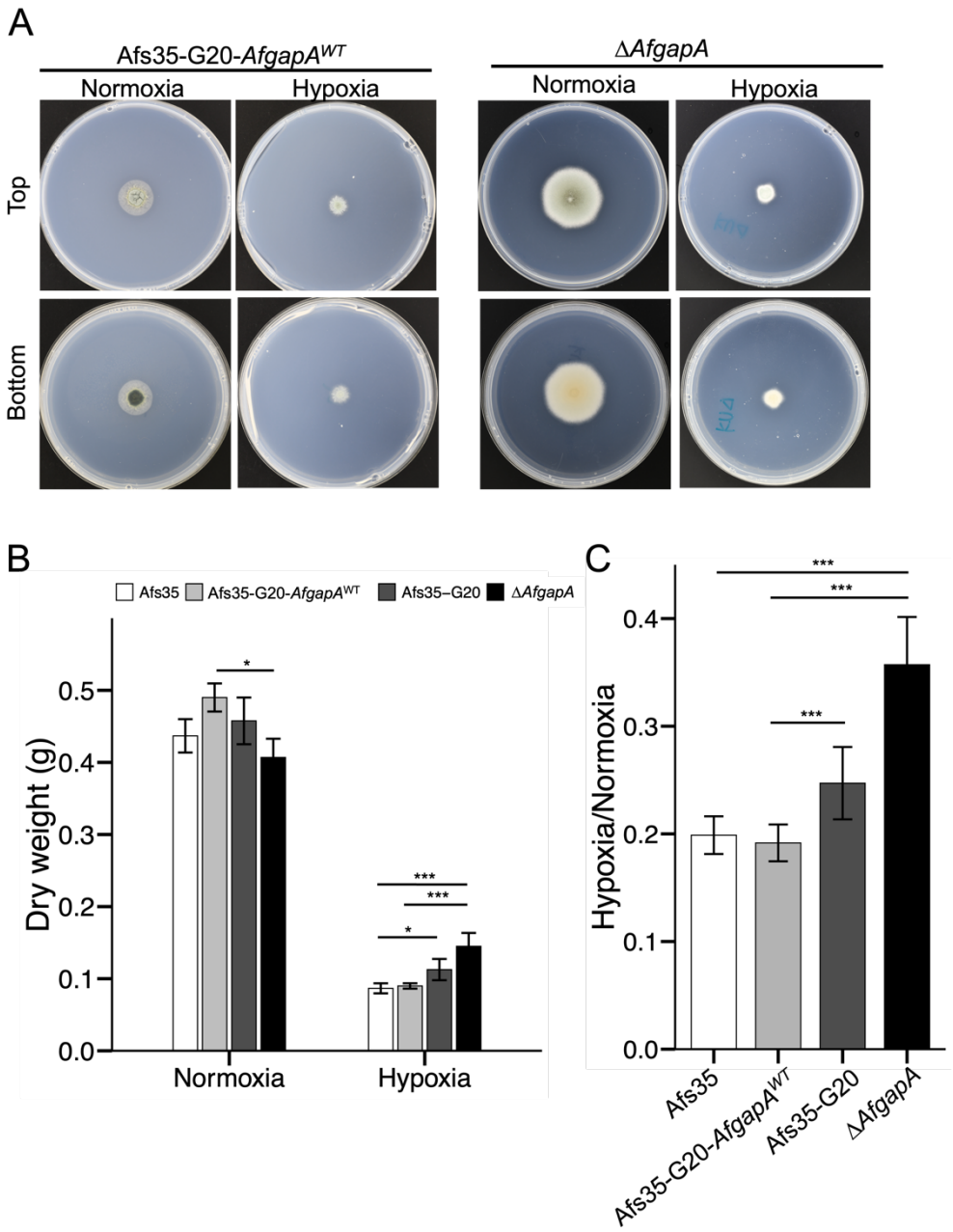

Fig. 19 Growth phenotypes of Afs35-G20-*AfgapA*^{WT} and Δ*AfgapA*. (A) Colony assays of Afs35, Afs35-G20-*AfgapA*^{WT}, Afs35-G20, and Δ*AfgapA* in hypoxia and normoxia. A total of 1×10^3 conidia for each strain were inoculated and grown on GMM for four days. (B) Dry weight of fungal biomass of Afs35, Afs35-G20-*AfgapA*^{WT}, Afs35-G20, and Δ*AfgapA* in hypoxia and normoxia. A total of 5×10^7 conidia were inoculated in 100 mL GMM and cultured for 48h, 37˚C, shaking at 200 rpm. (Data of Afs35 and Afs35-G20 were directly used from Fig. 6E) (C) The ratio of biomass in hypoxia to biomass in normoxia of Afs35, Afs35-G20-*AfgapA*^{WT}, Afs35-G20, and Δ*AfgapA*. Statistical analysis was performed using the Tukey HSD multiple comparison test (*, *p*-value < 0.05; **, *p*-value < 0.01; ***, *p*-value < 0.001).

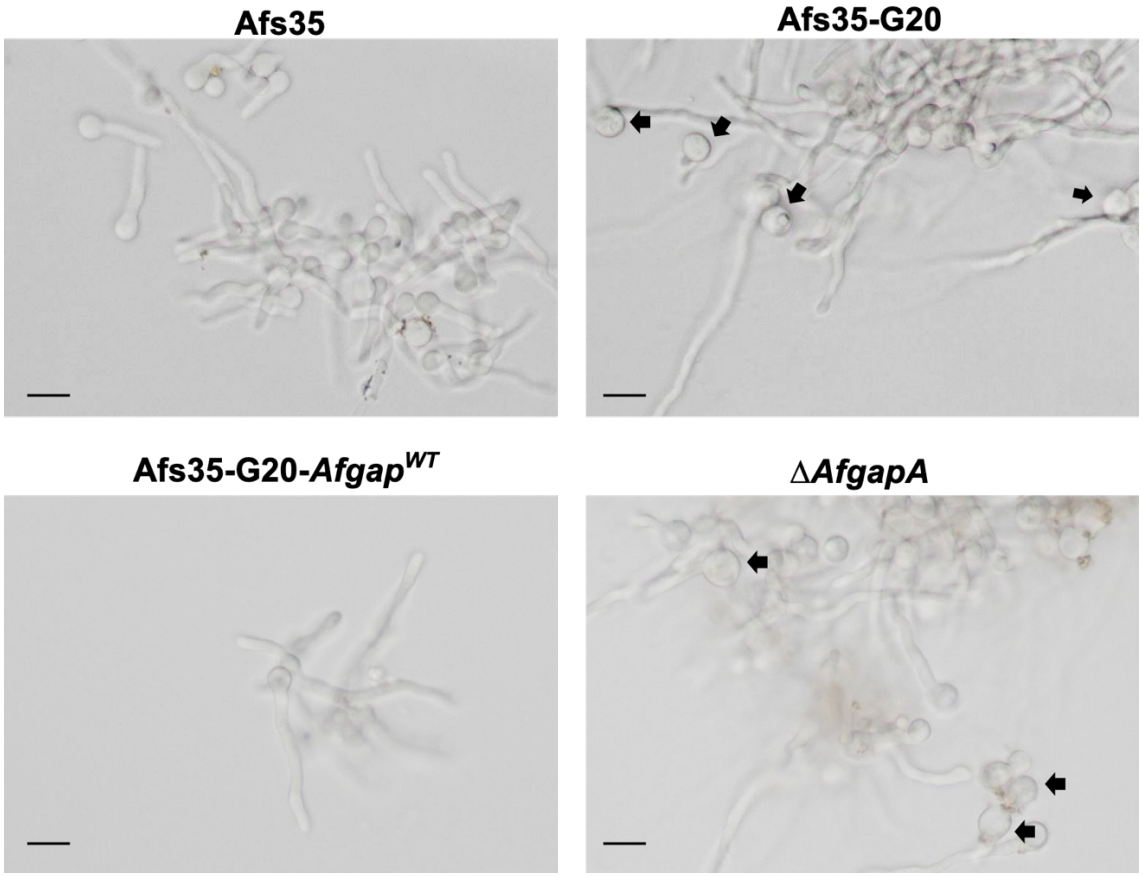

Fig. 20 Effect of *AfgapA* on conidia morphology during germination. Afs35-G20 and Δ*AfgapA* produced abnormally giant conidia during germination (black arrows). Scale bars indicate 10 μm.

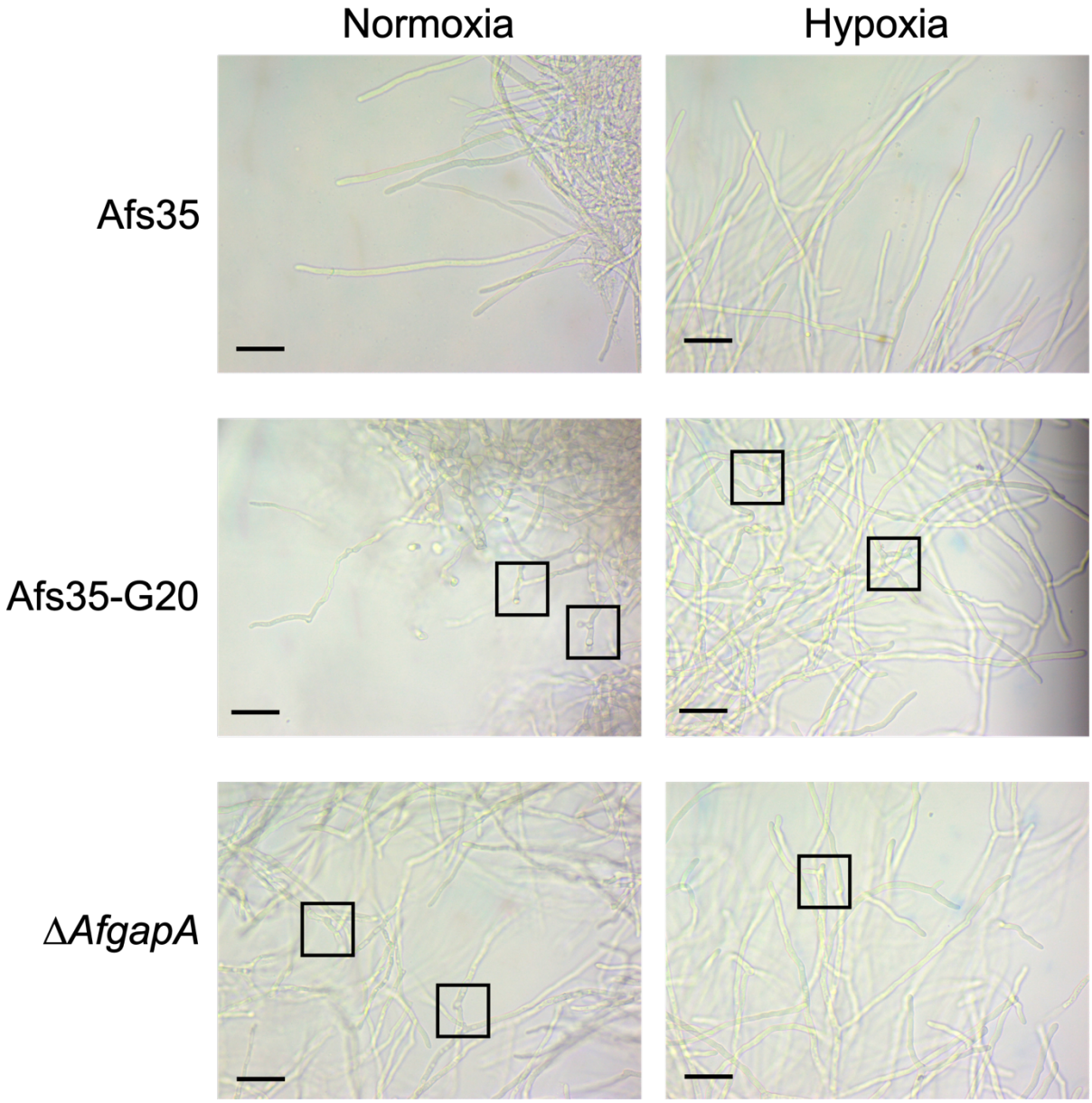

Fig. 21 Effect of *AfgapA* on the hyphal morphology in liquid culture under hypoxic and normoxic conditions, respectively. Abnormally swollen regions and apical branching are indicated with black boxes. Scale bars indicate 20 μm.

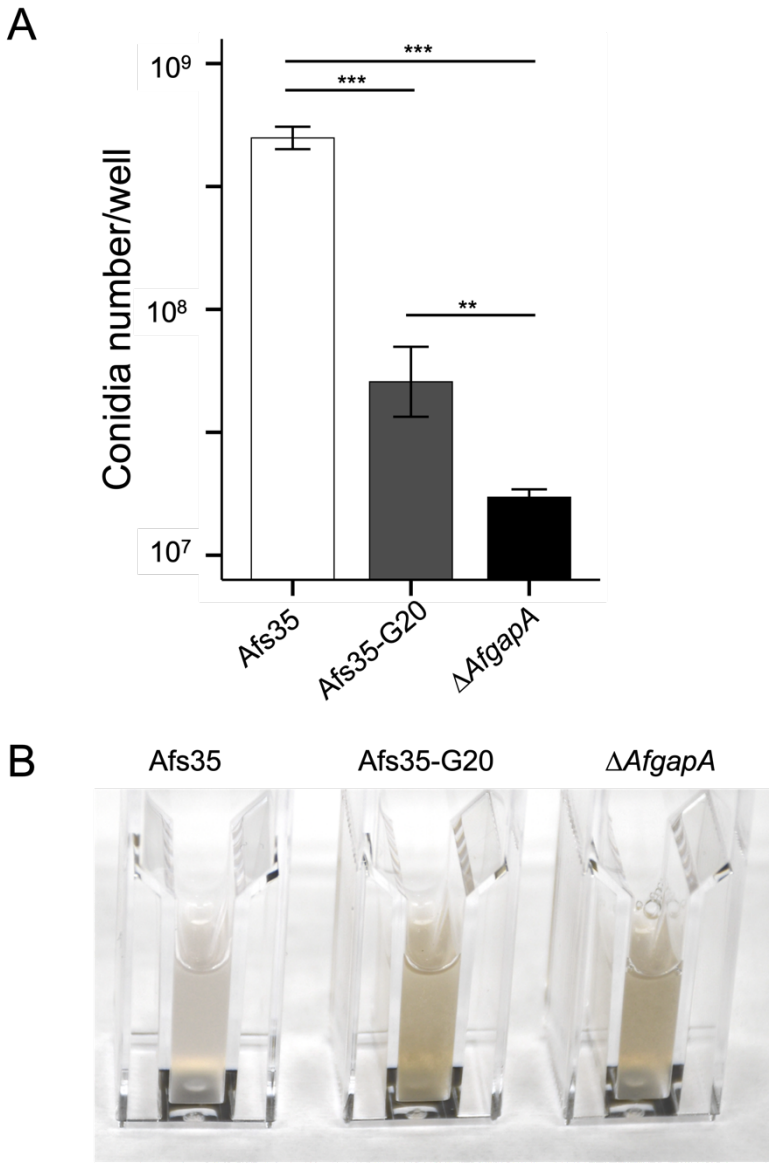

Fig. 22 Effect of *AfgapA* on conidiation and conidial pigmentation. (A) The number of conidia per well in Afs35, Afs35-G20 and Δ*AfgapA* after five days incubation at 37 °C. Statistical analysis was performed using the Tukey HSD multiple comparison test (**, *p*-value < 0.01; ***, *p*-value < 0.001). (B) Color of conidia in Afs35, Afs35-G20 and Δ*AfgapA*. 2×10^7 conidia are presented.

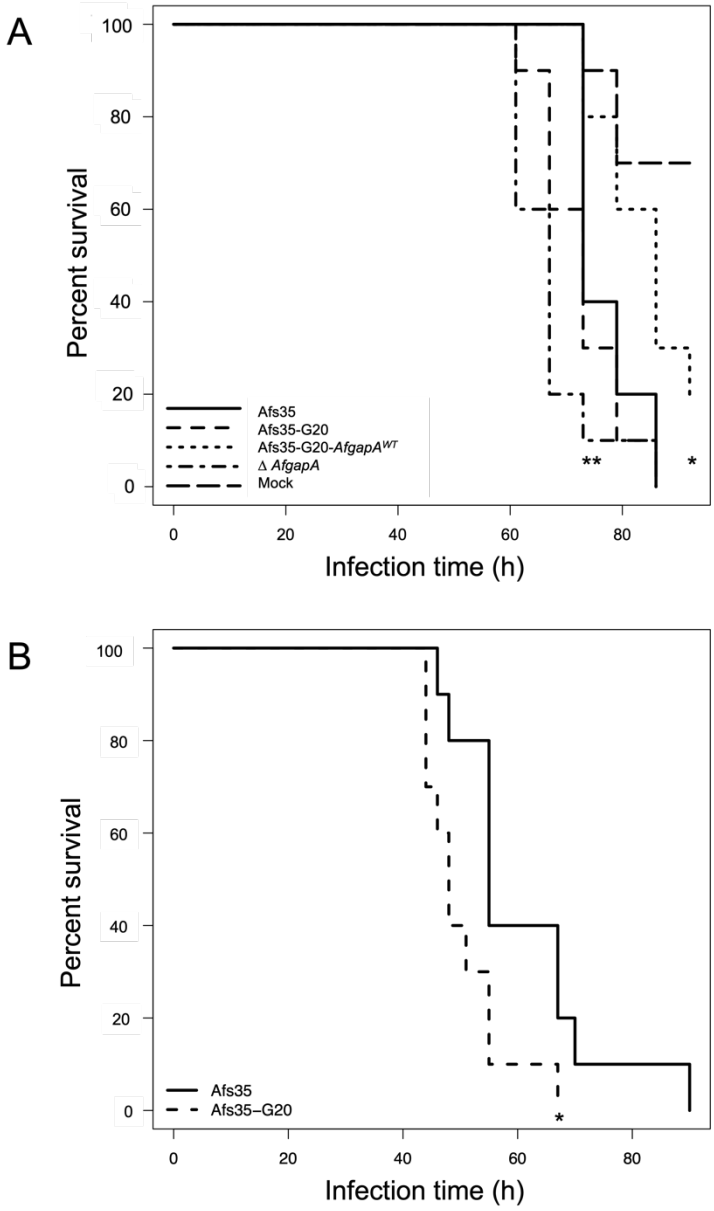

Fig. 23 Evaluation of virulence of *AfgapA* in silkworm infection model. (A) Survival rates of silkworms inoculated with Afs35, Afs35-G20-*AfgapA*^{WT}, Afs35-G20 and Δ*AfgapA* were evaluated (n = 10). A total of 1.5×10^5 conidia were infected for each silkworm. The difference of virulence level between Afs35 and Afs35-G20 was not significant (p = 0.2). Δ*AfgapA* exhibited higher virulence levels in the silkworm model (p = 0.009), while Afs35-G20-*AfgapA*^{WT}exhibited lower virulence than the wild type (p = 0.02). Mock (n = 10) as an uninfected group was also made. (B) The difference between Afs35 and Afs35-G20 was significant when 1.5×10^7 conidia were infected (p = 0.02). Statistical analysis was performed using a log-rank test (*, p-value < 0.05; **, p-value < 0.01).

Table 1 Three mutations identified in Afs35-G20

Gene ID	Position	Mutation	Consequence	Annotation
AfgapA (Afu3g09900)	Chr3, 2,540,500	SNP, T->G	Tyr757Ter	Ortholog(s) have GTPase activator activity
thtA (Afu1g03992)	Chr1, 1,150,600	2-base deletion, -GA	23 amino acids deletion from 664 to 686	Thermotolerance protein, essential for growth at high temperatures
dml1 (Afu1g15070)	Chr1, 4,049,579	SNP, G->A	synonymous	Protein dml1, putative

Table 2 Four strains further investigated in this study

Strain	Genotype
Afs35	*AfgapA,thtA*
Afs35-G20	$AfgapA^{Tyr757Ter}$, $thtA^{mut}$
Afs35-G20-$AfgapA^{WT}$	$AfgapA,thtA^{mut}$
Δ*AfgapA*	Δ*AfgapA,thtA*

Table 3 Antifungal susceptibility test of four strains generated in this study

	MCFG*	**CPFG**	**AMPH**	**5-FC**	**FLCZ**
Afs35	<0.015	0.25	1	64	>64
Afs35-G20	<0.015	0.25	1	64	>64
Afs35-G20-*AfgapA*^{WT}	<0.015	0.25	0.5	64	>64
Δ*AfgapA*	<0.015	0.25	1	64	>64

	ITCZ	**VRCZ**	**MCZ**
Afs35	0.5	0.5	2
Afs35-G20	0.25	0.5	2
Afs35-G20-*AfgapA*^{WT}	0.5	0.5	2
Δ*AfgapA*	0.5	0.5	2

*MCFG; micafungin; CPFG: caspofungin; AMPH: amphotericin B; 5-FC: 5-fluorocytosine; FLCZ: fluconazole
ITCZ: itraconazole; VRCZ: voriconazole; MCZ: miconazole

Table 4 Primers used for strain construction

no.	Primer	Sequence (5′-3′)*
1	3g09900-UF	cccctcctgcttcctgatccttaat
9	Hph-3g09900-UR	GGTGATATCGGCCTGAGTGGCCTCactgtgaaagaaaaactatgg
10	Hph-3g09900-DF	GTTGTCGACGGCCATCTAGGCCAGgatgattagcgcagcgtctaa
11	3g09900-DR_deletion	gatagagggcatgaatagtcaagtc
2	3g09900-sg5Mut-UR	tgtagatgctctcgacgcaggctgtaacattgttgctacagacat
3	3g09900-sg5Mut-M1F	atgtctgtagcaacaatgttacagcctgcgtcgagagcatctaca
4	3g09900-G_T-sg3Mut-M1R	tgagcactttagaaacattgaactggacatactcgagatcgagat
5	3g09900-G_T-sg3Mut-M2F	atctcgatctcgagtatgtccagttcaatgtttctaaagtgctca
6	Hph-3g09900-M2R	atatcggcctgagtggcctcaccgccgaagaagattcaga
7	Hph-3g09900-DF	tcgacggccatctaggccagatgagttgcgtctgcttttc
8	3g09900-DR	cttccaatggtggcaacctgcagtt
12	T7-sgRNA1-3g09900	TTCTAATACGACTCACTATAGTGTAGCAACAATGTTGCAACGTTTTAGAGCTAGA
13	T7-sgRNA2-3g09900	TTCTAATACGACTCACTATAGCACTTTAGAAACGTTAAATGTTTTAGAGCTAGA
14	Hph5	GAGGCCACTCAGGCCGATATCACC
15	Hph3	CTGGCCTAGATGGCCGTCGACAAC

*Uppercases and lowercases represent the sequences derived from plasmid pHph and *A. fumigatus* genome, respectively. Additional sequences for in vitro gRNA synthesis are underlined.

Table 5 Primers used for RT-PCR

Primer	Sequence (5′-3′)
act1-qF	GGTATCCACGTCACCACTTT
act1-qR	GGTACCACCAGACATGACAA
AfugapA_qF	GTCTTCATTACAAAGGCCGTGCTCG
AfugapA_qR	CTGCGCTAATCATCTTACCAGCCCT

Acknowledgments

I express my sincere thanks to Dr. Hiroki Takahashi for his kind instructions. I would like to thank Dr. Yoko Kusuya, Dr. Junichi Ishihara, and Dr. Takashi Umeyama (National Institute of Infectious Diseases) for their thoughtful discussion, Ryoko Mori and Getong Dao for their experimental assistance. This work was supported by JST SPRING, Grant Number JPMJSP2109. Additionally, I acknowledge the work of past and present members of the Division of Bio-resources.

References

Andreini C, Bertini I, Cavallaro G, et al (2008) Metal ions in biological catalysis: from enzyme databases to general principles. JBIC Journal of Biological Inorganic Chemistry 13:1205–1218. https://doi.org/10.1007/s00775-008-0404-5

Bankevich, A., Nurk S, Antipov D, Gurevich AA, et al (2012) SPAdes: a new genome assembly algorithm and its applications to single-cell sequencing. Journal of Computational Biology 19:455–477

Barker BM, Kroll K, Vödisch M, et al (2012) Transcriptomic and proteomic analyses of the *Aspergillus fumigatus* hypoxia response using an oxygen-controlled fermenter. BMC Genomics 13:62. https://doi.org/10.1186/1471-2164-13-62

Bat-Ochir C, Kwak J-Y, Koh S-K, et al (2016) The signal peptide peptidase SppA is involved in sterol regulatory element-binding protein cleavage and hypoxia adaptation in *Aspergillus nidulans*. Molecular Microbiology 100:635–655. https://doi.org/10.1111/mmi.13341

Bertuzzi M, van Rhijn N, Krappmann S et al (2021) On the lineage of *Aspergillus fumigatus* isolates in common laboratory use. Med Mycol 59:7–13. https://doi.org/10.1093/mmy/myaa075

Bien CM, Espenshade PJ (2010) Sterol Regulatory Element Binding Proteins in Fungi: Hypoxic Transcription Factors Linked to Pathogenesis. Eukaryotic Cell 9:352–359. https://doi.org/10.1128/EC.00358-09

Brakhage AA, Langfelder K (2002) Menacing Mold: The Molecular Biology of *Aspergillus fumigatus*. Annual Review of Microbiology 56:433–455. https://doi.org/10.1146/annurev.micro.56.012302.160625

Brakhage AA, Liebmann B (2005) *Aspergillus fumigatus* conidial pigment and cAMP signal transduction: significance for virulence. Medical Mycology 43:75–82. https://doi.org/10.1080/13693780400028967

Brunke S, Seider K, Fischer D, et al (2014) One small step for a yeast - microevolution within macrophages renders *Candida glabrata* hypervirulent due to a single point mutation. PLoS Pathogens 10:e1004478. https://doi.org/10.1371/journal.ppat.1004478

Butler G (2013) Hypoxia and gene expression in eukaryotic microbes. annual review of microbiology 67:291–312. https://doi.org/10.1146/annurev-micro-092412-155658

Cantelli G, Bateman A, Brooksbank C, et al (2022) The European Bioinformatics Institute (EMBL-EBI) in 2021. Nucleic Acids Research 50:D11–D19. https://doi.org/10.1093/nar/gkab1127

Carlsson P-O, Palm F, Andersson A, Liss P (2001) Markedly decreased oxygen tension in transplanted rat pancreatic islets irrespective of the implantation site. Diabetes 50:489–495.

https://doi.org/10.2337/diabetes.50.3.489

Castresana J (2000) Selection of conserved blocks from multiple alignments for their use in phylogenetic analysis. Molecular Biology and Evolution 17:540–552. https://doi.org/10.1093/oxfordjournals.molbev.a026334

Chang YC, Khanal Lamichhane A, Garraffo HM, et al (2014) Molecular mechanisms of hypoxic responses via unique roles of Ras1, Cdc24 and Ptp3 in a human fungal pathogen *Cryptococcus neoformans.* PLoS Genetics 10:e1004292. https://doi.org/10.1371/journal.pgen.1004292

Chen S, Zhou Y, Chen Y, Gu J (2018) fastp: an ultra-fast all-in-one FASTQ preprocessor. Bioinformatics 34:i884–i890. https://doi.org/10.1093/bioinformatics/bty560

de Valk HA, Meis JFGM, Curfs IM, et al (2005) Use of a novel panel of nine short tandem repeats for exact and high-resolution fingerprinting of *Aspergillus fumigatus* isolates. Journal of Clinical Microbiology 43:4112–4120. https://doi.org/10.1128/JCM.43.8.4112-4120.2005

DeLano W (2002) Pymol: An open-source molecular graphics tool. CCP4 Newsletter on protein crystallography 82–92

Denning DW (1998) Invasive aspergillosis. Clinical Infectious Diseases 26:781–803. https://doi.org/10.1086/513943

Dewhirst MW (1998) Concepts of oxygen transport at the microcirculatory level. Seminars in Radiation Oncology 8:143–150. https://doi.org/10.1016/S1053-4296(98)80040-4

Erecińska M, Silver IA (2001) Tissue oxygen tension and brain sensitivity to hypoxia. Respiration Physiology 128:263–276. https://doi.org/10.1016/S0034-5687(01)00306-1

Festa RA, Thiele DJ (2011) Copper: An essential metal in biology. Current Biology 21:R877–R883. https://doi.org/10.1016/j.cub.2011.09.040

Fillinger S, Chaveroche M-K, Shimizu K, et al (2002) cAMP and ras signalling independently control spore germination in the filamentous fungus *Aspergillus nidulans*. Molecular Microbiology 44:1001–1016. https://doi.org/10.1046/j.1365-2958.2002.02933.x

Fliesser M, Morton CO, Bonin M, et al (2015) Hypoxia-inducible factor 1α modulates metabolic activity and cytokine release in anti- *Aspergillus fumigatus* immune responses initiated by human dendritic cells. International Journal of Medical Microbiology 305:865–873. https://doi.org/10.1016/j.ijmm.2015.08.036

Fortwendel JR, Panepinto JC, Seitz AE, et al (2004) *Aspergillus fumigatus* rasA and rasB regulate the timing and morphology of asexual development. Fungal Genetics and Biology 41:129–139. https://doi.org/10.1016/j.fgb.2003.10.004

Fortwendel JR, Zhao W, Bhabhra R, et al (2005) A fungus-specific Ras homolog contributes to the hyphal growth and virulence of *Aspergillus fumigatus*. Eukaryotic Cell 4:1982–1989. https://doi.org/10.1128/EC.4.12.1982-1989.2005

Franzot SP, Mukherjee J, Cherniak R, et al (1998) Microevolution of a standard strain of *Cryptococcus neoformans* resulting in differences in virulence and other phenotypes. Infection and Immunity 66:89–97. https://doi.org/10.1128/IAI.66.1.89-97.1998

Grahl N, Dinamarco TM, Willger SD, et al (2012a) *Aspergillus fumigatus* mitochondrial electron transport chain mediates oxidative stress homeostasis, hypoxia responses and fungal pathogenesis. Molecular Microbiology 84:383–399. https://doi.org/10.1111/j.1365-2958.2012.08034.x

Grahl N, Puttikamonkul S, Macdonald JM, et al (2011) In vivo hypoxia and a fungal alcohol dehydrogenase influence the pathogenesis of invasive pulmonary Aspergillosis. PLoS Pathogens 7:e1002145. https://doi.org/10.1371/journal.ppat.1002145

Grahl N, Shepardson KM, Chung D, Cramer RA (2012b) Hypoxia and fungal pathogenesis: To air or not to air? Eukaryotic Cell 11:560–570. https://doi.org/10.1128/EC.00031-12

Hagiwara D, Arai T, Takahashi H, et al (2018a) Non-*cyp51A* Azole-Resistant *Aspergillus fumigatus* isolates with mutation in HMG-CoA Reductase. Emerging Infectious Diseases 24:1889–1897. https://doi.org/10.3201/eid2410.180730

Hagiwara D, Takahashi H, Takagi H, et al (2018b) Heterogeneity in pathogenicity-related properties and stress tolerance in *Aspergillus fumigatus* clinical isolates. Medical Mycology Journal 59:E63–E70. https://doi.org/10.3314/mmj.18-00007

Hagiwara D, Takahashi H, Watanabe A, et al (2014) Whole-genome comparison of *Aspergillus fumigatus* strains serially isolated from patients with aspergillosis. Journal of Clinical Microbiology 52:4202–4209. https://doi.org/10.1128/JCM.01105-14

Hagiwara D, Takahashi-Nakaguchi A, Toyotome T, et al (2013) NikA/TcsC histidine kinase is involved in conidiation, hyphal morphology, and responses to osmotic stress and antifungal chemicals in *Aspergillus fumigatus*. PLoS ONE 8:e80881. https://doi.org/10.1371/journal.pone.0080881

Hall A (1998) Rho GTPases and the actin cytoskeleton. Science 279:509–514. https://doi.org/10.1126/science.279.5350.509

Harispe L, Portela C, Scazzocchio C, et al (2008) Ras GTPase-activating protein regulation of actin cytoskeleton and hyphal polarity in *Aspergillus nidulans*. Eukaryotic Cell 7:141–153. https://doi.org/10.1128/EC.00346-07

Hillmann F, Linde J, Beckmann N, et al (2014) The novel globin protein fungoglobin is involved in low oxygen adaptation of *A spergillus fumigatus*. Molecular Microbiology 93:539–553. https://doi.org/10.1111/mmi.12679

Howard SJ, Cerar D, Anderson MJ, et al (2009) Frequency and evolution of azole resistance in *Aspergillus fumigatus* associated with treatment failure. Emerging Infectious Diseases 15:1068–1076. https://doi.org/10.3201/eid1507.090043

Jin JJ, Yu W bin, Yang JB, et al (2020) GetOrganelle: a fast and versatile toolkit for accurate *de novo* assembly of organelle genomes. Genome Biology 21:241. https://doi.org/10.1186/s13059-020-02154-5

Jumper J, Evans R, Pritzel A, et al (2021) Highly accurate protein structure prediction with AlphaFold. Nature 596:583–589. https://doi.org/10.1038/s41586-021-03819-2

Katoh K (2002) MAFFT: a novel method for rapid multiple sequence alignment based on fast Fourier transform. Nucleic Acids Research 30:3059–3066. https://doi.org/10.1093/nar/gkf436

Katoh K, Standley DM (2013) MAFFT Multiple Sequence Alignment Software Version 7: Improvements in Performance and Usability. Molecular Biology and Evolution 30:772–780. https://doi.org/10.1093/molbev/mst010

Klaassen CHW (2009) MLST versus microsatellites for typing *Aspergillus fumigatus* isolates. Medical Mycology 47:S27–S33. https://doi.org/10.1080/13693780802382244

Kowalski CH, Beattie SR, Fuller KK, et al (2016) Heterogeneity among isolates reveals that fitness in low oxygen correlates with *Aspergillus fumigatus* virulence. mBio 7:e01515-16. https://doi.org/10.1128/mBio.01515-16

Kroll K, Shekhova E, Mattern DJ, et al (2016) The hypoxia-induced dehydrogenase HorA is required for coenzyme Q10 biosynthesis, azole sensitivity and virulence of *Aspergillus fumigatus*. Molecular Microbiology 101:92–108. https://doi.org/10.1111/mmi.13377

Latgé J-P (2001) The pathobiology of *Aspergillus fumigatus*. Trends in Microbiology 9:382–389. https://doi.org/10.1016/S0966-842X(01)02104-7

Latgé J-P (1999) *Aspergillus fumigatus* and Aspergillosis. Clinical Microbiology Reviews 12:310–350. https://doi.org/10.1128/CMR.12.2.310

Latgé J-P, Beauvais A, Chamilos G (2017) The Cell Wall of the Human Fungal Pathogen *Aspergillus fumigatus*: Biosynthesis, Organization, Immune Response, and Virulence. Annual Review of Microbiology 71:99–116. https://doi.org/10.1146/annurev-micro-030117-020406

Latgé J-P, Chamilos G (2019) *Aspergillus fumigatus* and Aspergillosis in 2019. Clinical Microbiology Reviews 33:e00140-18. https://doi.org/10.1128/CMR.00140-18

Li H (2013) Aligning sequence reads, clone sequences and assembly contigs with BWA-MEM

Li H, Handsaker B, Wysoker A, et al (2009) The Sequence Alignment/Map format and SAMtools. Bioinformatics 25:2078–2079. https://doi.org/10.1093/bioinformatics/btp352

Li L, Stoeckert CJ, Roos DS (2003) OrthoMCL: Identification of Ortholog Groups for Eukaryotic Genomes. Genome Research 13:2178–2189. https://doi.org/10.1101/gr.1224503

Liu W, Xie Y, Ma J, et al (2015) IBS: an illustrator for the presentation and visualization of biological sequences. Bioinformatics 31:3359–3361.

https://doi.org/10.1093/bioinformatics/btv362

Majima H, Arai T, Kusuya Y, et al (2021) Genetic differences between Japan and other countries in *cyp51A* polymorphisms of *Aspergillus fumigatus*. Mycoses 64:1354–1365. https://doi.org/10.1111/myc.13370

Mariani V, Biasini M, Barbato A, Schwede T (2013) lDDT: a local superposition-free score for comparing protein structures and models using distance difference tests. Bioinformatics 29:2722–2728. https://doi.org/10.1093/bioinformatics/btt473

Matherne GP, Headrick JP, Coleman SD, Berne RM (1990) Interstitial Transudate Purines in Normoxic and Hypoxic Immature and Mature Rabbit Hearts. Pediatric Research 28:348–353. https://doi.org/10.1203/00006450-199010000-00010

Matsumoto Y, Sekimizu K (2019) Silkworm as an experimental animal for research on fungal infections. Microbiology and Immunology 63:41–50. https://doi.org/10.1111/1348-0421.12668

Mayorga ME, Timberlake WE (1992) The developmentally regulated *Aspergillus nidulans* wA gene encodes a polypeptide homologous to polyketide and fatty acid synthases. Molecular and General Genetics MGG 235:205–212. https://doi.org/10.1007/BF00279362

Norton TS, Fortwendel JR (2014) Control of ras-mediated signaling in *Aspergillus fumigatus*. Mycopathologia 178:325–330. https://doi.org/10.1007/s11046-014-9765-1

Ramil E, Agrimonti C, Shechter E, et al (2000) Regulation of the CYB2 gene expression: transcriptional co-ordination by the Hap1p, Hap2/3/4/5p and Adr1p transcription factors. Molecular Microbiology 37:1116–1132. https://doi.org/10.1046/j.1365-2958.2000.02065.x

Ries LNA, Steenwyk JL, de Castro PA et al (2019) Nutritional heterogeneity among *Aspergillus fumigatus* strains has consequences for virulence in a strain- and host-dependent manner. Front Microbiol 10:854. https://doi.org/10.3389/fmicb.2019.00854

Robinson NJ, Winge DR (2010) Copper Metallochaperones. Annual Review of Biochemistry 79:537–562. https://doi.org/10.1146/annurev-biochem-030409-143539

Scheffzek K, Ahmadian MR, Kabsch W, et al (1997) The Ras-RasGAP complex: Structural basis for GTPase activation and its loss in oncogenic ras mutants. Science 277:333–338. https://doi.org/10.1126/science.277.5324.333

Schrettl M, Beckmann N, Varga J, et al (2010) HapX-Mediated Adaption to Iron Starvation Is Crucial for Virulence of *Aspergillus fumigatus*. PLoS Pathogens 6:e1001124. https://doi.org/10.1371/journal.ppat.1001124

Shen W, Le S, Li Y, Hu F (2016) SeqKit: a cross-platform and ultrafast toolkit for FASTA/Q file manipulation. PLoS ONE 11:e0163962. https://doi.org/10.1371/journal.pone.0163962

Shepardson KM, Ngo LY, Aimanianda V, et al (2013) Hypoxia enhances innate immune activation to *Aspergillus fumigatus* through cell wall modulation. Microbes and Infection 15:259–269.

https://doi.org/10.1016/j.micinf.2012.11.010

Shimizu K, Keller NP (2001) Genetic Involvement of a cAMP-Dependent Protein Kinase in a G Protein Signaling Pathway Regulating Morphological and Chemical Transitions in *Aspergillus nidulans*. Genetics 157:591–600. https://doi.org/10.1093/genetics/157.2.591

Simmen H-P, Battaglia H, Giovanoli P, Blaser J (1994) Analysis of pH, pO2 and pCO2 in drainage fluid allows for rapid detection of infectious complications during the follow-up period after abdominal surgery. Infection 22:386–389. https://doi.org/10.1007/BF01715494

Siso MIG, Becerra M, Maceiras ML, et al (2012) The yeast hypoxic responses, resources for new biotechnological opportunities. Biotechnology Letters 34:2161–2173. https://doi.org/10.1007/s10529-012-1039-8

Som T, Kolaparthi VS (1994) Developmental decisions in *Aspergillus nidulans* are modulated by Ras activity. Molecular and Cellular Biology 14:5333–5348. https://doi.org/10.1128/mcb.14.8.5333-5348.1994

Stajich JE, Harris T, Brunk BP, et al (2012) FungiDB: an integrated functional genomics database for fungi. Nucleic Acids Research 40:D675–D681. https://doi.org/10.1093/nar/gkr918

Stamatakis A (2014) RAxML version 8: a tool for phylogenetic analysis and post-analysis of large phylogenies. Bioinformatics 30:1312–1313. https://doi.org/10.1093/bioinformatics/btu033

Stanke M, Schöffmann O, Morgenstern B, Waack S (2006) Gene prediction in eukaryotes with a generalized hidden Markov model that uses hints from external sources. BMC Bioinformatics 7:62. https://doi.org/10.1186/1471-2105-7-62

Studer L, Csete M, Lee S-H, et al (2000) Enhanced Proliferation, Survival, and Dopaminergic Differentiation of CNS Precursors in Lowered Oxygen. The Journal of Neuroscience 20:7377–7383. https://doi.org/10.1523/JNEUROSCI.20-19-07377.2000

Szewczyk E, Nayak T, Oakley CE, et al (2006) Fusion PCR and gene targeting in *Aspergillus nidulans*. Nature Protocols 1:3111–3120. https://doi.org/10.1038/nprot.2006.405

Takahashi-Nakaguchi A, Muraosa Y, Hagiwara D, et al (2015) Genome sequence comparison of *Aspergillus fumigatus* strains isolated from patients with pulmonary aspergilloma and chronic necrotizing pulmonary aspergillosis. Medical Mycology 53:353–360. https://doi.org/10.1093/mmy/myv003

Tanaka K, Nakafuku M, Satoh T, et al (1990) *S. cerevisiae* genes IRA1 and IRA2 encode proteins that may be functionally equivalent to mammalian ras GTPase activating protein. Cell 60:803–807. https://doi.org/10.1016/0092-8674(90)90094-U

Thorvaldsdottir H, Robinson JT, Mesirov JP (2013) Integrative Genomics Viewer (IGV): high-performance genomics data visualization and exploration. Briefings in Bioinformatics 14:178–192. https://doi.org/10.1093/bib/bbs017

Umeyama T, Hayashi Y, Shimosaka H, et al (2018) CRISPR/Cas9 Genome Editing To

Demonstrate the Contribution of Cyp51A Gly138Ser to Azole Resistance in *Aspergillus fumigatus*. Antimicrobial Agents and Chemotherapy 62:e00894-18. https://doi.org/10.1128/AAC.00894-18

Vaknin Y, Hillmann F, Iannitti R, et al (2016) Identification and Characterization of a Novel *Aspergillus fumigatus* Rhomboid Family Putative Protease, RbdA, Involved in Hypoxia Sensing and Virulence. Infection and Immunity 84:1866–1878. https://doi.org/10.1128/IAI.00011-16

van Belle H, Goossens F, Wynants J (1987) Formation and release of purine catabolites during hypoperfusion, anoxia, and ischemia. American Journal of Physiology-Heart and Circulatory Physiology 252:H886–H893. https://doi.org/10.1152/ajpheart.1987.252.5.H886

Wang Y, Boguski M, Riggs M, et al (1991) sar1, a gene from S*chizosaccharomyces pombe* encoding a protein that regulates ras1. Cell Regulation 2:453–465. https://doi.org/10.1091/mbc.2.6.453

Warn PA (2004) Effect of hypoxic conditions on in vitro susceptibility testing of amphotericin B, itraconazole and micafungin against *Aspergillus* and *Candida*. Journal of Antimicrobial Chemotherapy 53:743–749. https://doi.org/10.1093/jac/dkh153

Wartenberg A, Linde J, Martin R, et al (2014) Microevolution of *Candida albicans* in Macrophages Restores Filamentation in a Nonfilamentous Mutant. PLoS Genetics 10:e1004824. https://doi.org/10.1371/journal.pgen.1004824

Wery N (2014) Bioaerosols from composting facilities-a review. Frontiers in Cellular and Infection Microbiology 4:42. https://doi.org/10.3389/fcimb.2014.00042

Wezensky SJ, Cramer RA (2011) Implications of hypoxic microenvironments during invasive aspergillosis. Medical Mycology 49:S120–S124. https://doi.org/10.3109/13693786.2010.495139

Willger SD, Cornish EJ, Chung D, et al (2012) Dsc Orthologs Are Required for Hypoxia Adaptation, Triazole Drug Responses, and Fungal Virulence in *Aspergillus fumigatus*. Eukaryotic Cell 11:1557–1567. https://doi.org/10.1128/EC.00252-12

Willger SD, Puttikamonkul S, Kim K-H, et al (2008) A Sterol-Regulatory Element Binding Protein Is Required for Cell Polarity, Hypoxia Adaptation, Azole Drug Resistance, and Virulence in *Aspergillus fumigatus*. PLoS Pathogens 4:e1000200. https://doi.org/10.1371/journal.ppat.1000200

Wu M-Y, Mead ME, Lee M-K, et al (2018) Systematic Dissection of the Evolutionarily Conserved WetA Developmental Regulator across a Genus of Filamentous Fungi. mBio 9(4):e01130-18. https://doi.org/10.1128/mBio.01130-18

Yu G, Smith DK, Zhu H, et al (2017) GGTREE: an R package for visualization and annotation of phylogenetic trees with their covariates and other associated data. Methods in Ecology and

Evolution 8:28–36. https://doi.org/10.1111/2041-210X.12628

Yu Y, Wolf AK, Thusek S, et al (2021) Direct visualization of fungal burden in filamentous fungus-infected silkworms. Journal of Fungi 7:1–18. https://doi.org/10.3390/jof7020136

Zhao S, Gibbons JG (2018) A population genomic characterization of copy number variation in the opportunistic fungal pathogen *Aspergillus fumigatus*. PLOS ONE 13:e0201611. https://doi.org/10.1371/journal.pone.0201611

Supplementary tables and figures

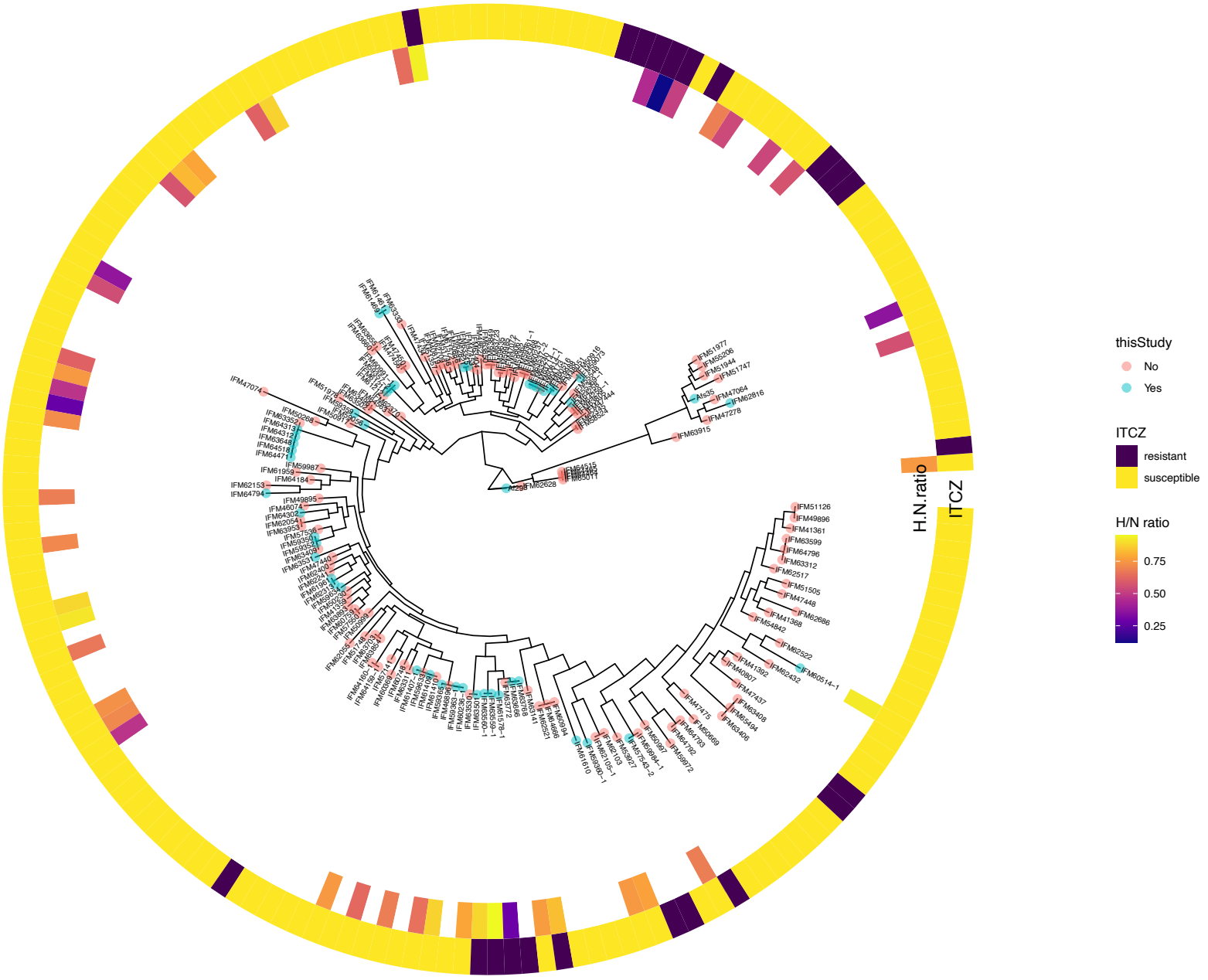

Fig. S1 Whole-genome SNP-based phylogenetic tree. Af293 as reference.

```
# -*- coding: utf-8 -*-
import os
import sys
import re
from Bio.Seq import Seq
from fuzzysearch import find_near_matches

f=open("/Users/bian/Documents/Af/single_isolation/genomeseq/
primers", "Ur")
primers={}       #2A-RV:seqr,2A-FW-SQ:seq2,2B-RV...
for line in f:
    name,pseq = line.rstrip().split()
        primers[name]=pseq
f.close()

boundary_seqs={} #RV:complementary
rule={'A':'T', 'C':'G', 'T':'A', 'G':'C'}
for key in primers:
    boundary_seqs[key]=primers[key]
        if "RV" in key:
        primers[key]
                seq_list=[rule[i] for i in primers[key]];
seq="".join(seq_list)

boundary_seqs[key]=str(Seq(primers[key]).reverse_complement())


strs={"2A":"GA","2B":"AG","2C":"CA","3A":"TCT","3B":"AAG","3C":"TAG"
,"4A":"TTCT","4B":"CTAT","4C":"ATGT"}
strsL=["2A","2B","2C","3A","3B","3C","4A","4B","4C"]

def getindex(fs,rs,seq):
        matchlistf=find_near_matches(fs,seq,max_l_dist=1)
        matchlistr=find_near_matches(rs,seq,max_l_dist=1)
        matchlist = matchlistf + matchlistr
        #return matchlist
        data=[]
        for i in matchlist:     #find min dist primer index.
i:'Match(start=2', ' end=6', ' dist=1)'
                a=re.split(",",str(i))
                startindex=re.split("=",str(a[0]))[1]
                dist=re.split("[=,)]",str(a[2]))[1]
                data.append((startindex,dist))
                data.sort(key=lambda x: x[1])    #data:
[(startindex,dist),(...]
        return data

def getSTRnum(data,seq,tandem):
        ind=int(data[0][0])
        inter=seq[ind-500:ind+500]
        ind1st=inter.index(strs[tandem])

        s1=len(strs[tandem]);s2=1;s3=0;s2max=s2      #s1:str
length; s2：occurrence time; s3:try - 1
```

```
        while len(inter[ind1st:ind1st+s3])<len(inter[ind1st:]):
                while
inter[ind1st+s3+s2*s1:ind1st+s3+s2*s1+s1]==strs[tandem]:       #get
length s1 string
                        s2+=1
                if s2>s2max:
                        s2max=s2
                s2=0
                s3+=1
        #return inter
        return s2max


def getSeq(fa):
        f=open(fa,"Ur")
        seq="";seq_rev=""
        for line in f:
                line=line.rstrip()
                seq+=line       #
        for i in seq:
                if i in rule:
                        seq_rev+=rule[i]
        seq_rev = seq_rev[::-1]
        f.close()
        return seq,seq_rev

def result():
        fa = sys.argv[1]
        out = []
        print "\t".join(strsL)
        for tandem in strsL:
                fs=boundary_seqs[tandem+"-FW-SQ"];
rs=boundary_seqs[tandem+"-RV"]
                #print tandem,getindex(fs,rs,seq)
                #break
                seq,seq_rev = getSeq(fa)
                if getindex(fs,rs,seq):
                        seq2 = seq
                elif getindex(fs,rs,seq_rev):
                        seq2 = seq_rev
                else:
                        out.append("-")
                        continue
                idx = getindex(fs,rs,seq2)
                out.append(str(getSTRnum(idx,seq2,tandem)))
                #print
"\t".join([fa,tandem,str(getSTRnum(idx,seq2,tandem))])
        print "\t".join(out)
result()
```

Fig. S2 extract_STR_from_assembly.py

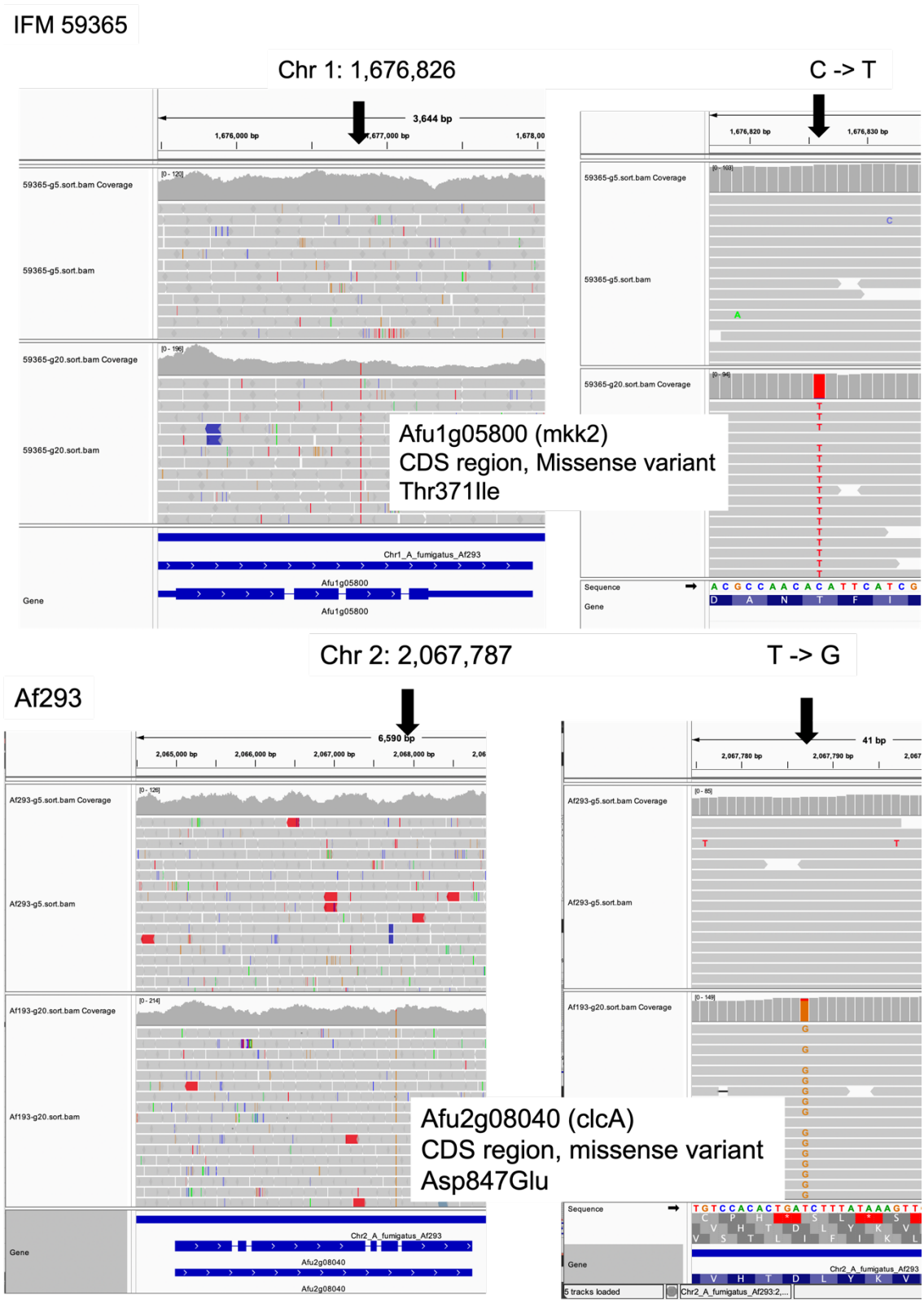

Fig. S3 Two SNPs identified in IFM 59365-G20 and Af293. Both were missense mutations in the CDS region of the respective genes.

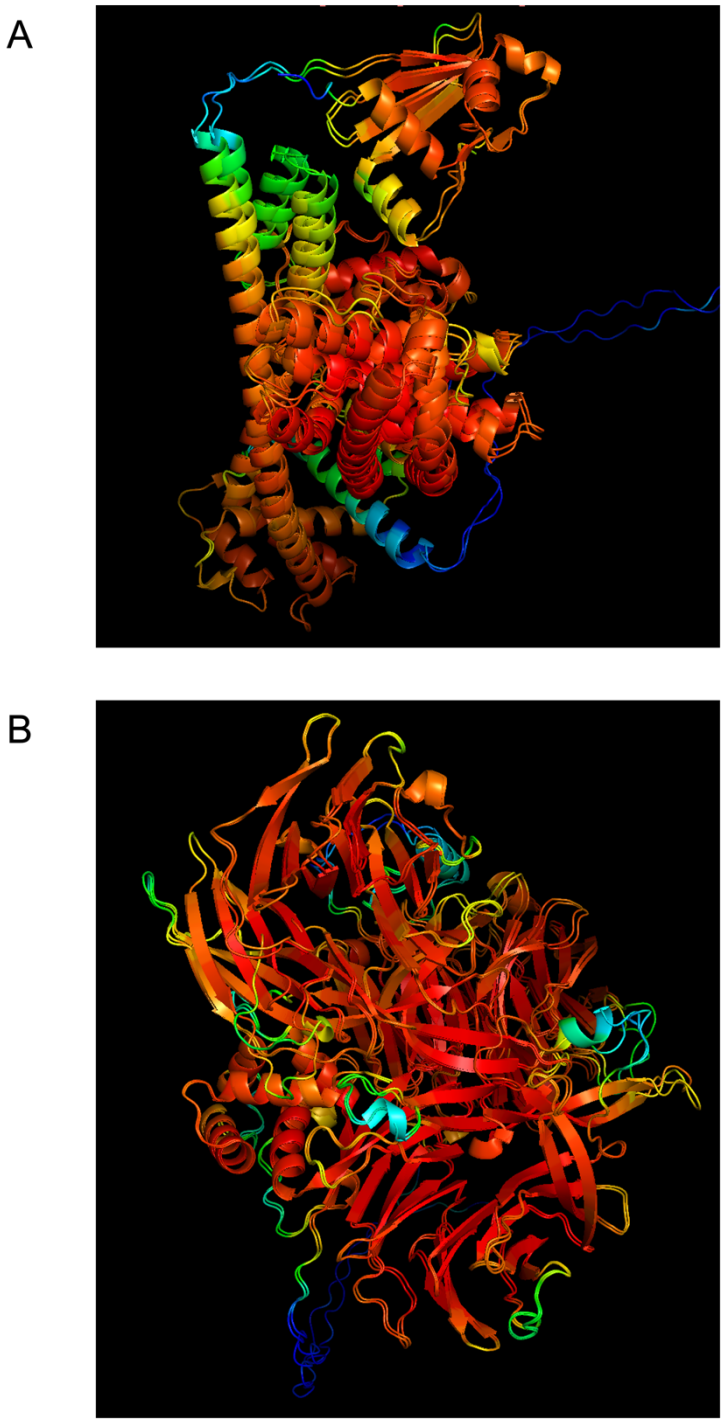

Fig. S4 pLDDT visualization for AfGapA (A) and THTA (B). Red color indicates higher pLDDT value (source code was from https://github.com/CYP152N1/plddt2csv).

Table S1 56 strains investigated in this study

Strain*	Isolation date	Source	Azoles application	Azole susceptibility			H/N diameter ratio
				ITCZ	VRCZ	PCZ	
Af293							0.75
Afs35							0.36
IFM 62821	9/2012			0.5	0.25		0.64
IFM 63345	7/2014			>8	2	>8	0.93
IFM 63666	11/2015			1	2	1	0.76
IFM 63768	1/2016			8	>8	8	0.83
IFM 59350	3/2009			0.5	0.5		0.88
IFM 59360	9/2009		VRCZ: 12m	1	1		0.77
IFM 60814	9/2011	(Hagiwara et al. 2018a)		0.5	0.5	1	0.84
IFM 63240	11/2014	(Hagiwara et al. 2018a)	VRCZ: 38m	>8	>8	4	0.12
IFM 63537	7/2015	(Hagiwara et al. 2018a)	VRCZ: 46m	>8	8	8	0.45
IFM 63714	4/2016	(Hagiwara et al. 2018a)	VRCZ: 51m	>8	8	4	0.51
IFM 64173	5/2016	(Hagiwara et al. 2018a)	VRCZ: 56m	>8	8		0.62
IFM 59363	1/2010			0.5	0.5		0.65
IFM 60236	1/2011			0.5	1		0.87
IFM 59357	7/2009			1	0.5		0.82
IFM 60991	12/2011			0.5	1		0.78
IFM 63559	6/2014			2	>8	4	0.95
IFM 63560	6/2015		VRCZ: 12m	8	>8	4	0.88
IFM 57543	11/2007			4	0.25	>8	0.68
IFM 58401				0.5	0.5		0.37
IFM 59073	3/2010	(Hagiwara et al. 2018b)		0.5			0.53

(Table S1 continued)

IFM 59365		(Hagiwara et al. 2018b)	0.5	0.5	0.79
IFM 59359		(Zhao and Gibbons 2018)	0.5	0.5	0.37
IFM 59056		(Hagiwara et al. 2018b)	1	1	0.55
IFM 59777			1	1	0.57
IFM 61118			0.5	0.5	0.77
IFM 62516			0.5	0.5	0.58
IFM 61407	5/2012	(Hagiwara et al. 2018b)	0.25	0.25	0.75
IFM 64518			0.5	0.5	0.28
IFM 61461	7/2012		0.25	0.5	0.87
IFM 55369		(Hagiwara et al. 2018b)	0.5	0.25	0.57
IFM 59365			0.5	0.5	0.68
IFM 59634	10/2010		1	0.5	0.48
IFM 59988			1	0.5	0.54
IFM 62816			1	4	0.56
IFM 60514	4/2011		0.5		0.92
IFM 61578	10/2012		4	0.25	0.29
IFM 62115			0.5	0.5	0.78
IFM 61610			1	0.5	0.75
IFM 58026			1	1	0.74
IFM 61961	5/2013		1	0.5	0.73
IFM 64313			0.5	0.5	0.61
IFM 64312			0.5	0.5	0.75
IFM 63648			0.5	0.5	0.48
IFM 64471			0.5	0.5	0.72
IFM 63501			1	2	0.78
IFM 61469	8/2012		0.25	0.5	0.61
IFM 59352			1	1	0.91

(Table S1 continued)

IFM 64302		0.5	1	0.71
IFM 64794		0.5	1	0.68
IFM 62313	12/2013	0.125	0.25	0.71
IFM 60516	5/2011	1	1	0.68
IFM 63531		1	0.5	0.66
IFM 61409	6/2012	0.25	0.25	0.63
IFM 61211	11/2011	0.25	0.5	0.57

* Same colored strains indicate that they were isolated from the same patient

Table S2 Genomic information

Strain	# of reads after filtration	Mapping rate (bwa-MEM, Af293)	Assembly (SPAdes)				
			#scaffolds	min_len	avg_len	max_len	N50
Af293-G5	7,894,642	99.78%	414	502	69,421	720,602	259,136
Af293-G10	9,551,326	99.87%					
Af293-G15	14,067,151	99.87%					
Af293-G20	13,019,372	99.81%	709	500	40,552	1,101,615	231,566
Afs35-G5	8,723,727	98.78%	554	505	50,753	835,217	195,804
Afs35-G10	7,982,546	98.88%	702	500	40,032	648,140	165,248
Afs35-G15	10,189,874	98.89%					
Afs35-G20	12,272,583	98.81%					
IFM 58401-G5	8,592,259	98.42%					
IFM 58401-G10	10,695,323	98.36%					
IFM 58401-G15	10,663,951	98.37%					
IFM 58401-G20	10,726,137	98.48%					
IFM 59365-G5	7,732,721	98.11%	473	505	60,445	896,043	219,123
IFM 59365-G10	11,086,355	98.09%					
IFM 59365-G15	4,241,459	98.13%					
IFM 59365-G20	8,704,678	98.23%	551	500	51,337	542,460	154,277
IFM 63240-G5	10,004,503	98.24%	429	501	66,050	828,680	291,612
IFM 63240-G20	7,283,973	98.24%	488	504	57,592	572,074	192,824
IFM 63559-G5	8,907,945	98.88%	386	500	72,225	716,524	268,639
IFM 63559-G20	14,494,756	97.79%	336	521	85,098	802,977	275,247

Table S3 STR generated from the assembly data

Strain	2A	2B	2C	3A	3B	3C	4A	4B	4C
Af293-g0	26	18	18	46	20	23	11	10	8
Af293-g5	26	18	18	26	20	23	11	10	8
Af293-g20	26	18	18	25	20	24	11	10	8
KU-g0	14	21	8	18	9	10	8	10	6
KU-g5	14	21	8	24	9	10	8	10	6
KU-g20	14	21	8	25	9	10	8	10	6
59365-g5	11	12	15	18	15	13	15	10	5
59365-g20	11	12	15	18	15	13	15	10	5
63240-g5	21	20	16	37	13	25	10	12	8
63240-g20	18	23	14	34	26	25	10	11	8
63559-1-g5	19	22	23	26	13	15	10	9	5
63559-1-g20	18	26	28	25	12	23	13	9	8